NASA Technical Memorandum 84911

Evaluation of a Flow Direction Probe and a Pitot-Static Probe on the F-14 Airplane at High Angles of Attack and Sideslip

Terry J. Larson

March 1984

NASA
National Aeronautics and
Space Administration

NASA Technical Memorandum 84911

Evaluation of a Flow Direction Probe and a Pitot-Static Probe on the F-14 Airplane at High Angles of Attack and Sideslip

Terry J. Larson
Ames Research Center, Dryden Flight Research Facility, Edwards, California 93523

1984

NASA
National Aeronautics and
Space Administration
Ames Research Center
Dryden Flight Research Facility
Edwards, California 93523

SUMMARY

The accuracy of air-data measurements made with a hemispherical flow-angularity probe and with a fuselage-mounted pitot-static-pressure probe has been evaluated as part of a more general high-angle-of-attack flight-test program conducted with the F-14 airplane at the Dryden Flight Research Facility of NASA Ames Research Center. The evaluations were made at high flow angles, using a calibrated combined pitot-static and flow-angularity probe for reference measurements and another reference probe mounted in a fuselage pod. Data are presented for angles of attack up to 63°, angles of sideslip from -22° to 22°, and for Mach numbers from approximately 0.3 to 1.3. Flow-angle measurements made with the hemispherical flow-angularity probe at high angles of attack and sideslip typically were in error by more than 2°. These errors result from a ack of the precise pressure measurements needed to determine flow direction accurately and from pneumatic-lag effects. Pressure measurements with the pitot-static-pressure probe resulted in very inaccurate data above a Mach number of 0.87. The probe measurements also showed great sensitivity to changes in angles of attack and sideslip.

INTRODUCTION

It is probable that air-data sensor systems have been developed to such an extent that the accuracy of measurements made with conventional sensors is taken for granted by flight-test engineers and pilots. Although this assumption may be warranted when these systems are used under normal flight conditions, it is far less justifiable at the high angles of attack and sideslip at which modern aircraft are flown — for example, the F-14, F-15, F-18, and the X-29 research airplane. (The X-29 is described in ref. 1.)

The F-14 high-angle-of-attack control-system investigation at the Dryden Flight Research Facility (ref. 2) provided a concomitant opportunity to evaluate the measuring performance of a hemispherical flow-angularity probe and a fuselage-mounted pitot-static-pressure probe at high flow angles. Determining flow-angles by measuring pressure is of interest because of the rapidly varying pressures associated with dynamic maneuvers that involve large angles of attack and sideslip. Since fuselage-mounted pitot-static probes present measurement problems even under benign flow conditions (especially at supersonic speeds) (ref. 3), it is important that their performance be evaluated at high flow angles.

The sensor evaluations reported here are based on reference measurements made with a calibrated noseboom probe, which provided pitot-static-pressure and flow-angle measurements (using vanes), and with a reference probe located below the nose of the fuselage, which also measured flow angle. Although the reference measurements are not necessarily error-free, especially at large flow angles, they are nevertheless more accurate than the sensors that were evaluated and thus provide at least a good qualitative standard.

This paper presents examples of sensor data that illustrate the deficiencies of the test sensors when used at high angles of attack and sideslip. Data are shown for angles of attack to 63°, at angles of sideslip from -22° to 22°, and at Mach numbers from 0.3 to 1.3.

SYMBOLS

AICS	air inlet control system
ARI	aileron-rudder interconnect
IR	infrared
K	calibration factor dependent on Mach number
M	Mach number
M_{pI}	Mach-number parameter defined by $(p_1 + p_2 + p_4 + p_5)/4p_3$
M_{pII}	Mach-number parameter defined by $(p_4 + p_5)/2p_3$
M_{pIII}	Mach-number parameter defined by $(p_1 + p_2)/2p_3$
M_{pIV}	Mach-number parameter defined by $(p_2 + p_3)/2p_1$
p	static pressure, N/cm^2 (lb/ft^2)
p_t	stagnation pressure, N/cm^2 (lb/ft^2)
$p_1, p_2, \ldots, p_5$	pressure measured at five ports of ARI probe (fig. 3)
SPS	samples per second
S_1	forward set of two static pressure sources on AICS probes (fig. 3)
S_2	aft set of the two static pressure sources on AICS probes (fig. 3)
t	time, sec
α	angle of attack, deg
α_{pI}	angle-of-attack parameter defined by $4(p_1 - p_2)/(p_1 + p_2 + p_4 + p_5)$
α_{pII}	angle-of-attack parameter defined by $(p_1 - p_2)/p_3$
α_{pIII}	angle-of-attack parameter defined by $(p_1 - p_2)/[(p_3 - p_1) + 0.5\,(p_1 - p_2)]$
α_{pIV}	angle-of-attack parameter defined by $(p_1 - p_2)/[p_3 - 0.5\,(p_4 + p_5)]$
β	angle-of-sideslip, deg
β_{pI}	angle-of-sideslip parameter defined by $(p_4 - p_5)/[p_3 - 0.5\,(p_1 + p_2)]$

β_{pII}	angle-of-sideslip parameter defined by $(p_4 - p_5)/[p_3 - p_4 + 0.5\,(p_4 - p_5)]$
δ	change in quantity, to approximate its differential
Δ	correction in quantity following delta, e.g., $\Delta\alpha_{ARI} = (\alpha_\infty - \alpha_{ARI})$ is the correction to the ARI probe angle of attack

Subscripts:

ARI	refers to the aileron-rudder interconnect flow-angularity probe
AICS	refers to measurements with one of the two air inlet control system pitot-static probes
IR	refers to measurement with the vane-type angularity probe mounted on the infrared scanner pod
max	maximum
o	ordinate intercept of curves shown in figure 31
∞	free stream, obtained from noseboom reference probe system

AIR-DATA SENSORS

Several air-data sensors are used to provide pitot-static-pressure and flow-angularity measurements for the aircraft. Two of the primary sensors are evaluated in this paper. One, the aileron-rudder interconnect (ARI) probe, senses pressures from five orifices in a hemispherical probe; the pressures are used by two computers (ARI alpha and beta) to determine angles of attack and sideslip. The other sensor is a pitot-static-pressure probe called the air-inlet control system (AICS) probe. The ARI probe is shown installed on the nose of the F-14 in figure 1. Figure 2 shows the AICS probe that was mounted on the left side of the fuselage. Note the presence of the gun fairing upstream of the probe – it is a possible major source of interference in the probe measurements. The spin canard normally is not an interference source, for it is closed during flight except during spin tests. Another AICS probe was located in the same position on the right side of the fuselage (there is no gun fairing on the right side). The AICS probes have two sets of orifices, as shown in figure 3(b). The forward sets, designated S_1, are manifolded and used as an input to the air-data computer. Each S_2 set is plumbed to a separate AICS computer.

The ARI probe (fig. 3(a)) was modified for flight testing to provide angle-of-sideslip measurements in addition to angle-of-attack measurements. The modification consisted of installing a pneumatic averager which allows both absolute and differential pressure measurements to be made from common pressure ports. Such measurements are required by the algorithms used by the computers; with the exception of a constant, the algorithms are identical to the α_{pIV} and β_{pI} parameters discussed in this paper.

The performance of the two sensors was evaluated using two calibrated, reference air-data probe systems. Figures 4 and 5 show the reference probes. The noseboom probe (fig. 4) provided test reference measurements of pitot-static pressure and angles-of-attack and sideslip. The second probe was installed under the fuselage on the pod that houses the IR scanner; it is thus referred to as the IR probe. It consisted of vanes for making flow-angularity measurements in two body-planes (see figs. 5 and 6). Basic dimensions of the two reference probes are shown in figure 6.

The performance of the ARI probe with the probe installed on the aircraft nose, as well as on the IR pod (with the vane probe removed) was evaluated. The data presented in this paper were obtained with the probe's centerline aligned parallel with the aircraft waterline.

INSTRUMENTATION

Accurate force-balance, absolute-pressure transducers were used to measure pitot-static pressure. The same type transducers were used to measure the ARI pressures, p_1 through p_5. The accuracies of these measurements varied somewhat, but the largest uncertainties in the recorded measurements were within ± 0.014 N/cm^2 (± 3 lb/ft^2). A differential-pressure transducer was used to measure the difference between S_1 and S_2 pressures (fig. 3(b)) to determine the AICS S_1 static pressure. The pressure uncertainty associated with this transducer was ± 0.0014 N/cm^2 (± 0.3 lb/ft^2). All of the pressures were recorded to a resolution better than 0.0005 N/cm^2 (0.1 lb/ft^2). Indicated values of angles of attack and sideslip from the vane systems were all recorded to an accuracy and resolution of better than 0.1°.

Data were recorded on board the airplane on magnetic tape, using a pulse-code modulation (PCM) data system; they were then telemetered to the ground station. Real-time monitoring was achieved by using a cathode ray tube (CRT) display and strip-chart recorder.

SENSOR EVALUATION

Angle-of-attack and angle-of-sideslip data from the nose-mounted ARI probe were compared with corrected data from the IR-pod-mounted vane probe as reference conditions; on the other hand, data obtained when the ARI probe was mounted on the IR pod (with the vane probe removed) were compared with the noseboom-vane data as reference. Hence, it should be kept in mind that both the aircraft nose and the IR pod were used as test-sensor locations, as well as reference sensor locations. Pitot-static pressure data from the AICS probe were compared with the corrected measurements from the noseboom.

Corrections to the noseboom measurements were provided by calibrations from Grumman Aircraft Company. Static pressures were corrected for position errors as functions of Mach number for all Mach numbers, and as functions of angles of attack for Mach numbers less than 0.4. Angle-of-attack corrections were made for pitch velocity, upwash, boom bending and offset, and fuselage bending. Sideslip corrections were made for roll and yaw velocities. The IR-pod-mounted vane probe was calibrated at Dryden, using the noseboom vanes for reference measurements. The appendix describes the calibration procedure.

It was not practical to estimate the uncertainties in the reference pitot-static measurements because the effects of large flow angles on these measurements are not fully known. Likewise, the pneumatic lag is not accurately known. Nevertheless, it is believed that the reference pressures are reasonably accurate at flow angles less than about 10° and that the accuracy decreases, especially above M = 0.4, as flow angle increases. For example, the pitot-static pressure uncertainties are both approximately 1 percent at low flow angles, but are believed to be well over 10 percent at the higher angles. Uncertainties in the reference angles of attack and sideslip for the noseboom are believed to be generally within 1°, except at large flow angles and large Euler angle rates. The IR-pod-mounted reference vane probe angles have an additional 1° of calibration uncertainty.

ARI probe data were obtained from the ARI alpha and beta computers. The angle-of-attack algorithm is $\alpha = (p_1 - p_2)/K(p_3 - p_{4,5})$ (ref. 4) where $p_{4,5}$ is an average pressure derived from orifices 4 and 5 as determined by use of the pneumatic averager. Angle of sideslip is determined by a similar algorithm (ref. 4). The K term is a calibration factor; although known to vary with Mach number, it is assigned a constant value for the computers. Values of angle of attack and sideslip obtained from the computers were appropriately corrected for pitch, roll, and yaw velocities.

As mentioned earlier, an ARI probe identical to the one mounted on the nose was installed on the IR pod (with the vane probe removed) and evaluated. The reason was to provide reference measurements of angles of attack and sideslip that could be used in calibrating the nose-mounted ARI probe. The IR-pod-mounted probe was first calibrated against data from the reference test noseboom before the nose-mounted ARI probe was installed. This procedure resulted from a requirement of the ARI flight-test program that the flight demonstration be conducted using the ARI probe instead of the flight-test noseboom. However, the calibration of the IR-pod-mounted probe was unsuccessful and hence the IR-pod-mounted vane probe was installed and subsequently calibrated for use in obtaining reference measurements.

During the unsuccessful attempts to calibrate the ARI probe, two modifications of the ARI probe system were made and investigated. In both modifications, the pneumatic averager was removed in an attempt to improve system accuracies, and another measurement was substituted for sensing the average "static" pressure required in the α_{pIV} or the β_{pI} algorithm (i.e., $0.5(p_4 + p_5)$ in α_{pIV} and $0.5\ (p_1 + p_2)$ in β_{pI}). In one modification, the S_1 static pressure was used from the AICS probes; in the other, ports 4 and 5 of the ARI probe were manifolded to provide the measurement. Note that in the latter modification it was not possible to determine the angle of sideslip by using the ARI probe, since the pressure difference between orifices 4 and 5 are needed for the determination. Evaluation of these modified ARI system configurations is also included in this paper.

The evaluation presented herein of the AICS and ARI sensors is in terms of general sensor characteristics with respect to reference flow conditions, especially, for example, angle of attack, rather than in terms of complete analysis of calibration procedures and accuracies. A complete assessment is not possible from the results of the present study because of unknowns in the accuracies of the noseboom reference data, against which all of the other probes discussed in this paper were either directly or indirectly calibrated.

Pull-up and sideslip maneuvers were flown to obtain data at various angles of attack and sideslip. At the higher Mach numbers, split-S and descending turns were used to obtain data at the higher angles of attack; sideslips were difficult to

perform at constant angles of attack, especially at the higher angles of attack. Because the data presented in this paper were obtained primarily under transient conditions, they demonstrate the effects of dynamic maneuvers on the measurements. Some acceleration runs were also made to investigate Mach-number effects on the measurements.

The data discussed below, although not inclusive of all the acquired data, serve as selected representative results of the sensor evaluations and as such illustrate salient characteristics of the measurements.

RESULTS AND DISCUSSION

The performance evaluation of the ARI and AICS sensors is discussed in three parts: (1) flow-angle measurements from the nose-mounted ARI probe; (2) flow-angle measurements from the modified ARI configuration installed on the IR pod; and (3) the stagnation static-pressure measurements from the two AICS probes.

ARI Probe (Nose Installation)

A time history of a typical maneuver flown to assess the angle-of-attack measurement performance of the ARI probe is shown in figure 7. Note that from an initial value of 0.60, Mach number decreased to a value of about 0.10 near the peak angle of attack of 43°. The latter portion of the Mach number time history (after $t \approx 13$ sec) is not accurate, however, because the noseboom reference static pressure is not adequately corrected for position error as a function of angle of attack. For example, no corrections are made when the Mach number is greater than 0.4. It is seen that the angle of attack decreases very rapidly (at a rate of about 15°/sec) after the maximum angle of attack is obtained. This portion of the maneuver, which is typical of all of the angle-of-attack maneuvers investigated, provides a means of evaluating the pneumatic response of the pressure measurements from the ARI probe. The individual ARI pressures vary substantially during the time history, a result of both the angle-of-attack variation and the descending turn that was flown.

Figure 8 is a plot of ARI-determined angle of attack against the reference angle of attack for the maneuver just discussed (fig. 7). In figure 8, and in subsequent figures where it is pertinent, the data sample rate, in samples per second (SPS), is shown. A fairly linear relationship exists between the ARI and reference angles of attack for the increasing angle-of-attack points (fig. 8). The decreasing points show a nonlinear relationship, however, and, more importantly, disagree with the other points by at least 6° for some angles above 20°.

A number of factors were investigated in efforts to account for the discrepancies in the angle of attack shown in figure 8. These factors were (1) variation of the algorithm used by the ARI computer with Mach number; (2) errors in pitching-velocity correction; (3) low values of the quantity $p_3 - [(p_4 + p_5)/2]$, which is in the denominator of the ARI alpha-computer algorithm; (4) pneumatic lag; and (5) effects of the pneumatic averager. In considering factor (1), the algorithm used by the ARI alpha computer has a constant calibration factor K: $\alpha = (p_1 - p_2)/K(p_3 - p_{4,5})$. However, according to reference 4, K is not constant but varies by about 16 percent throughout the Mach number range. It is found that at an angle of attack of 30°, there can be a 2.4° error at certain Mach numbers, assuming that K is set at an average value. At

the Mach numbers flown in the maneuver under discussion, however, K should have been approximately constant, and, therefore, factor (1) cannot significantly account for the discrepancies noted in figure 8.

The error in pitch-velocity corrections (factor 2) for determining angle of attack can be large, as can errors in roll and yaw velocity corrections for determining angles of sideslip. These errors are consequences of errors in the true velocity, a term that appears in the denominator of the correction terms; this is especially true at low velocities. At high angles of attack, it is known that velocities computed from the reference noseboom measurements can be much too low (e.g., see fig. 7). Therefore, the corrections can be greatly exaggerated. For the data in figure 7, the pitch-velocity corrections to angle of attack were considerably less than 1° when angle of attack was decreasing. Some of the increasing angle of attack points were associated with somewhat larger corrections in the high-angle-of-attack region of the maneuver, but analysis shows that the pitch-velocity corrections did not significantly account for the noted discrepancies.

Factor (3) can have significant effects at large angles of attack, low Mach numbers, and high altitudes. The minimum value of $[p_3 - 0.5(p_4 + p_5)]$ is about 0.3 N/cm^2 (60 lb/ft^2), which occurred at the peak angle of attack (fig. 8). A 0.01 N/cm^2 (2 lb/ft^2) error in this quantity is equivalent to 1.5° error in angle of attack for this condition. Values of this quantity that are considerably lower than 0.3 N/cm^2 (60 lb/ft^2) have been noted in similar maneuvers. This factor, therefore, appears to be a major contributor to the discrepancies observed in figure 8.

In the interest of better understanding the source or sources of error (exclusive of the ARI alpha computer) that result in the discrepancies in the ARI-determined and reference angles of attack shown in figure 8, the pressure-angle-of-attack parameters, α_{pI} through α_{pIV}, are plotted in figure 9 for the same maneuver. These parameters, of course, reflect pressure measurements from the ARI sensor. Before continuing the error discussion, however, the application of these parameters in determining angle of attack must be considered. For example, the investigated α_{pI}, and α_{pII} parameters exhibit very little sensitivity to angle of attack variations and are, therefore, impractical for use in determining angle of attack. The other quantities show good sensitivity to angle-of-attack variations, however, and the α_{pIV} parameter yields a very linear relationship between ARI and reference angles of attack up to an angle of about 40°. The relationship for α_{pIII} parameter taken from reference 4 is very nonlinear at angles above about 26°. The data show that the largest discrepancies between increasing and decreasing angle-of-attack points for α_{pIII} and α_{pIV} parameters are associated with the highest angle-of-attack change rates. However, it was first necessary to examine lag effects on individual pressures — with the help of figure 7 — before it was decided that the discrepancy between the increasing and decreasing points results in the correct sign. In other words, the sign of the discrepancy is maneuver-dependent. For this maneuver, figure 7 indicates that the data that would be most affected by lag are those obtained after the maximum angle of attack is attained.

Figures 8 and 9 show that the results from the ARI alpha computer are in disagreement with the α_{pIV} pressure data as far as the discrepancy between increasing and decreasing angle-of-attack points are concerned. This disagreement can be attributed to a difference between computed values of the $0.5\ (p_4 + p_5)$ term, for

which the pressures are measured by individual pressure transducers, and the sensed value of $p_{4,5}$, using the pneumatic averager from the ARI alpha computer. Or it can be simply attributed to differences in pressure measurements between the transducers used in the parameter measurements and those of the computer. This analysis makes it clear that it is difficult to measure flow angles at high angles of attack to an accuracy of 1° or 2°, using the ARI-probe system, especially during dynamic maneuvers. The reasons are two-fold: the requirement that pressure measurements be very accurate and the effects of pneumatic lag.

Figure 10 shows a similar maneuver, except that it begins at Mach 0.9, the highest initial Mach number used for these tests. Again, large variations in the ARI-probe pressures resulted. For this case, however, no appreciable differences were noted between the increasing and decreasing angle-of-attack points, as shown in figure 11. In general, the higher Mach number runs produced more consistent data. However, again the α_{pIV} parameter data, as shown in figure 12, disagree with the results from the ARI alpha computer, indicating mismatched angles; there is also evidence of pneumatic lag.

As already indicated, the ARI alpha computer does not account for any sideslip effects when determining the angle of attack. Figure 13 shows that at small angles of attack, sideslip effects – at least for the range shown – are inconsequential at low Mach numbers (as indicated by the flat relationship of $\Delta\alpha_{ARI}$ and β_∞). Although the data are limited at the higher angles, there appears to be a significant sideslip effect, that is, the relationship between $\Delta\alpha_{ARI}$ and β_∞ has a discernible slope. Figure 14 shows that at higher Mach numbers, angle-of-sideslip effects are present in the ARI probe angle-of-attack data, even at low angles of attack.

Figure 15 shows sideslip corrections required of the ARI beta computer as a function of sideslip angle for various angles of attack and Mach number ranges. Figures 15(a) and 15(b) indicate that the corrections vary nonlinearly with angle of sideslip at low Mach numbers and at moderate angles of attack. However, the variation is linear for low angles of attack and high Mach numbers, as shown by figure 15(f). Much scatter exists in the data for the higher angles of attack (figs. 15(c) through 15(e)). There is also a significant difference between increasing and decreasing angle-of-sideslip points, especially at the higher angles of attack. However, the rate of change in sideslip angle was as high as 10°/sec for this maneuver.

Two sideslip parameters, β_{pI} and β_{pII}, are shown in figure 16. These parameters are constructed in a manner similar to those for the angle-of-attack parameters (α_{pIV} and α_{pIII}). The data correspond to the same times as the data in figures 15(b), 15(d), and 15(f). Recall that figure 15 shows a nonlinear relationship between the ARI-probe beta-computer measurements and true sideslip. Figure 16(a), however, which corresponds to the same maneuver shown in figure 15(b), shows that the transducer measurements for the decreasing sideslip points result in a linear relationship, indicating that the ARI-probe-computer values are less accurate. In comparison, some of the increasing sideslip points in figure 16(a) show nonlinearity and at least as many discrepancies as the ARI-probe-computer values. However, these discrepancies are probably a result of pressure lag rather than transducer errors. Note, for example, that the sideslip rate was much more rapid for the increasing sideslip points than for the decreasing points. Figures 16(b) and 16(c) show that the sideslip parameter data for these runs do not provide any better sideslip information than does the ARI-probe computer, again probably because of pneumatic lag. In summary, the same

general conclusions stated for the ARI-probe angle-of-attack measurements are applicable to ARI probe angle-of-sideslip measurements because of the similarity in the measurements.

ARI Probe (IR Pod Installation)

Flow angle measurements. - Typical results of the angle-of-attack measuring performance of the ARI-probe installed on the IR pod are presented in figures 17 and 18. The performance of the probe when the S_1 static pressure source from the AICS probes is substituted, as an input to the ARI-probe alpha and beta computers, for the usual static pressure source incorporating the pneumatic averager, is shown in figure 17. Several differences from the performance of the nose-installed ARI probe are noted. Noteworthy of these are that the ARI-computer angle of attack is not linear with angle of attack, and the difference between increasing and decreasing angle of attack points have the opposite sign from that observed for the nose installation (compare fig. 17(b) with fig. 8)). Also, these differences are quite large for this relatively high-Mach-number case, in contrast to the ARI nose-installation data for $M_{max} \approx 0.90$.

The performance of the probe for an angle of attack maneuver when the two ARI sideslip ports (4 and 5) were manifolded and used as a substitute "static"-pressure source for the ARI alpha computer is shown in figure 18. Although a more linear relationship results than when the AICS pressure source was used, large differences between increasing and decreasing points again occur.

Typical angle-of-sideslip measuring performance of the ARI probe mounted on the IR pod and using the S_1 static-pressure source from the AICS probes is shown in figure 19 for two maneuvers at different Mach numbers (0.6 and 0.9). A nonlinear relationship between the ARI-beta-computer angles and angle of sideslip results, but no appreciable Mach-number effects are evident.

From the above discussion, it can be concluded that removing the pneumatic averager had no beneficial effect on the performance of the ARI computers in measuring angles of attack and sideslip.

The α_{pI} and α_{pII} parameters measured when the pneumatic averager was operational are shown in figures 20(a) and 20(b) for a maneuver that resulted in extreme free-stream angles of attack. It is concluded from these plots that both parameters are entirely inadequate for determining angle of attack under these conditions. On the other hand, the α_{pIV} parameter (fig. 20(d) produces reasonable results for free-stream angle of attack up to about 40°. This corresponds to about 33° of local angle of attack (i.e., the angle of attack at the IR-pod-mounted probe) as can be seen from the calibration curve shown in figure 28 (discussed in the appendix). However, the values become asymptotic near a free-stream angle of attack of 49° (42° local angle of attack). Below 49°, the values approach negative infinity, and above 49° they approach positive infinity. This occurs, not surprisingly, because the denominator of α_{pIV} results in values that pass through zero near 49°. The effect of pressure lag is evident over the higher-angle-of-attack region.

The α_{pIII} parameter offers no improvement, as seen in figure 20(c). In fact it has a smaller definitive angle-of-attack range and becomes asymptotic near a free-stream angle of attack of only 40° (33° local angle of attack). Also, the lag effects are even more predominant for this parameter. The results in figure 20

clearly indicate the limitations of the ARI-probe-type sensor for measuring very high flow angles using the flow parameters considered in this paper. An alternative method that could provide more accurate solutions at high angles is one planned for air-data extraction using the shuttle entry air-data system (SEADS) pressure measurements, which are described in reference 5. In that method, a batch-filter technique is used to solve the "aerodynamic state vector" assuming a Newtonian pressure model.

Mach number determination. - The determination of Mach number by using the ARI probe installed on the IR pod was also investigated. Typical results obtained during an acceleration test are shown in figure 21. All four Mach-number parameters investigated showed adequate sensitivity to Mach numbers at numbers below 0.8, but they were only slightly sensitive to Mach number in the range of 0.8 to 1.3. Included in the figures for comparison are the ratios of static-to-stagnation pressure, for flow without position errors, plotted against Mach number. The parameter M_{pIV} results in improved sensitivity to Mach number, but also demonstrates unwanted sensitivity to angle of attack. Figure 22 illustrates that all four parameters, however, are sensitive to angle of attack at a Mach number of 0.4 and that M_{pIV} is the most sensitive parameter at the lower angles. It is concluded that the ARI probe mounted on the IR pod can be used to determine Mach number, using the Mach-number parameters investigated, but only at Mach numbers less than 0.8 and only if angles of attack and sideslip are known.

AICS Probes

The stagnation-pressure and static-pressure measurement performance of the AICS probes was evaluated in terms of Mach number and flow angles (see figs. 23 through 27).

The variation of $p_t/p_{t_{AICS}}$ with Mach number for both the left and right probes is shown in figure 23(a). Excessive scatter, commencing at $M \approx 0.87$, is evident in the data. The left probe results in considerably more scatter than the right probe at supersonic speeds. Because the scatter cannot be accounted for by transducer errors, it may very well have been a result of flow disturbances caused by the gun fairing upstream of the probe (recall that there is no gun fairing on the right side of the F-14 fuselage; see fig. 2).

Figure 23(b) shows the variation of p_∞/p_{AICS} versus Mach number for the S_2 static-pressure measurement of both probes. Only small scatter — and thus small variation of error — are indicated for Mach numbers between 0.60 and 0.87. However, much greater scatter is evident outside this range, especially at high Mach numbers. These results are not surprising because it is known that the transonic and supersonic pitot-static measuring performance of probes mounted on the sides of fuselages are affected by complex flow-interference phenomena and by reflected shocks (ref. 3).

The variations of $p_{t_{AICS}}/p_{t_\infty}$ and p_{AICS}/p_∞ with angle of attack near $M = 0.3$ are plotted in figure 24. (Note that in fig. 24, as well as in subsequent figures related to this subject, the pressure ratios are reciprocals of those presented in fig. 23 — a result of a change in data processing.) The variation with angle of attack for all of the AICS-probe pressure sources is similar. The S_1 pressures result in the largest errors. Similar plots, but for data at higher Mach numbers (near 0.6), are shown in figure 25. It is seen in figure 25(a) that stagnation pressure determined by the left probe (gun-fairing side of the fuselage) is much more sensitive to angle of

attack than that determined by the right probe. Subsequently, stagnation-pressure measurements from the right probe were substituted for stagnation-pressure measurements from the left probe as inputs to the air-data computer for conducting other flight tests with this airplane.

In analyzing the M = 0.6 static-pressure data (fig. 25(b)), it must be remembered that no corrections were made to the noseboom reference static pressures for position error as a function of angle of attack at that Mach number. Assuming that the noseboom static-pressure correction is positive and increases with angle of attack, as it is known to do at lower Mach numbers, then the AICS static-pressure error is even larger than that depicted in figure 25(b). The S_2 static pressure source from the right probe is seen to be slightly more sensitive to angle of attack than is the left probe. However, the S_2 source for both probes is much less sensitive to angle of attack than is the S_1 manifolded source, which results in a 24 percent decrease with respect to the noseboom reference static-pressure over the 40° angle-of-attack range shown.

Variations of $p_{t_{AICS}}/p_{t_\infty}$ and p_{AICS}/p_∞ with true angle of sideslip are shown in figures 26 and 27 for Mach numbers of 0.3 and 0.6, respectively. The AICS probe stagnation pressures are little affected by sideslip angle for the angles shown. However, the AICS-probe static pressures result in significant asymmetric variations for the higher Mach number test. The S_1 manifolded source results in the largest changes, which amount to 10 percent over the angle-of-sideslip range shown (figure 27(b)).

CONCLUSIONS

This evaluation of the measurement performance of a hemispherical, flow-angularity pressure probe and of a fuselage-mounted pitot-static probe flown at high flow angles on an F-14 aircraft permits the following conclusions:

1. The algorithm used by the computer for the hemispherical, flow-angularity probe (the ARI probe) results in a linear relationship with local angle of attack up to an angle of about 33°. However, at an angle of attack of about 42°, the algorithm is discontinuous because its denominator approaches zero. Other investigated algorithms were less useful.

2. Measurements of individual ARI pressures indicate that the ARI computers do not measure the same values, either because of the mechanization of the pneumatic averager or because of differences in the transducer measurements.

3. Angle-of-sideslip measurements with the computers for the ARI probe resulted in errors that varied nonlinearly with sideslip for some flight conditions. Independent measurements of the pressures from the ARI probe did not always result in more accurate measurements than those achieved with the computer, presumably because of the effects of pneumatic lag.

4. Pneumatic lag, which can cause errors of several degrees during dynamic maneuvers, and the need for very accurate pressure measurements at high flow angles, precludes the attainment of accurate flow-angle measurements with the ARI-probe system, as presently mechanized, throughout the flight envelope of the airplane.

5. No marked improvement was achieved in the measurement of angle of attack when the ARI-probe system was modified to eliminate the pneumatic averager.

6. Mach-number parameters were investigated that allow measurements of an IR-pod-mounted ARI probe to be used for determining free-stream Mach number. This effort was successful only for Mach numbers less than 0.8 and only if angles of attack and sideslip were known.

7. Stagnation-pressure measurements made with the pitot-static probes (AICS) mounted on the sides of the fuselage resulted in inaccurate data at Mach numbers above 0.87. The left probe exhibited more sensitivity to angle of attack than did the right probe, probably because of the gun fairing upstream of the probe on the left side of the fuselage (there is no fairing on the right side).

8. Static-pressure measurements made with the AICS probes also resulted in inaccurate data at Mach numbers above 0.87. The S_2 static-pressure source for both probes is much less sensitive to angle of attack than is the S_1 manifolded static-pressure source, which showed a 24 percent decrease with respect to the noseboom reference static-pressure over a 40° angle-of-attack range at M = 0.6. The S_1 static-pressure source also exhibited a 10 percent variation for a 26° angle-of-sideslip range at the same Mach number.

Ames Research Center
Dryden Flight Research Facility
National Aeronautics and Space Administration
Edwards, California, April 11, 1983

REFERENCES

1. DeMeis, Richard: Forward-Swept Wings and Supersonic Zip. High Technology, vol. 2, no. 1, Jan./Feb. 1982, pp. 33-40.

2. Gera, J.; Wilson, R. J.; Enevoldson, E. K.; and Nguyen, L. T.: Flight Test Experience With High-Control System Techniques on the F-14 Airplane. AIAA Paper 81-2505, Las Vegas, Nev., Nov. 1981.

3. Huffman, G. David: Theory, Performance and Design of Flow Direction and Mach Number Probes. Air Force Armament Laboratory, AFATL-TR-81-44, Apr. 1981.

4. Model 858 Flow Angle Sensors. Bulletin 1014, Rosemount Inc., Minneapolis, Minn., 1974.

5. Wolf, Henry; Pruett, Dave; and Martin, Henry: Shuttle Entry Air Data System Simulation Program (SEADSIM) – Program Description and User's Manual. AMA Report No. 81-8, Analytical Mechanics Associates, Inc., Hampton, Va., May 1981.

APPENDIX — CALIBRATION OF THE IR-POD-MOUNTED VANE PROBE

The IR-pod-mounted vane probe was calibrated for free-stream angle of attack and sideslip using the test noseboom vane measurements for references.

Figure 28 shows a set of measurements taken during an angle-of-attack maneuver at low speed and with near 0° of sideslip. Both angle-of-attack measurements (test and reference) were corrected for pitch rate. It was found that a second-degree, least-squares-curve fit of the data is representative of data from similar runs, regardless of the Mach number (highest Mach number tested was 0.9), as long as the angle of sideslip was close to 0°. For other sideslip angles, a correction was necessary, as seen from figure 29. It was decided that a single sideslip correction curve based on the low-angle-of-attack data (fig. 29(a)) would be adequate for all angles of attack, even though some of the higher-angle-of-attack data (fig. 29(b)) indicate a smaller slope. The resulting equation, then, is

$$\alpha_\infty = 7.60 + 1.141\alpha_{IR} - 0.0052(\alpha_{IR})^2 - 0.135\beta_{IR} \text{ deg}$$

A more complex calibration was required for the IR-pod-mounted probe sideslip measurements. Figure 30 shows that although linear curves can be drawn through the data, a strong dependence on angle of attack exists. The intercepts and slopes of these curves for the different angles of attack are plotted against angle of attack in figure 31. Straight lines have been fitted through the points to allow the development of the following algorithm:

$$\beta_\infty = \beta_{IR} + 0.560\alpha_{IR} - (0.0087\alpha_{IR} + 0.197)\beta_{IR} - 0.15 \text{ deg}$$

The accuracies of the flow equations, judging by the scatter in the data, are estimated to be about $\pm 1°$ and do not account for systematic errors in the test noseboom flow-angle measurements.

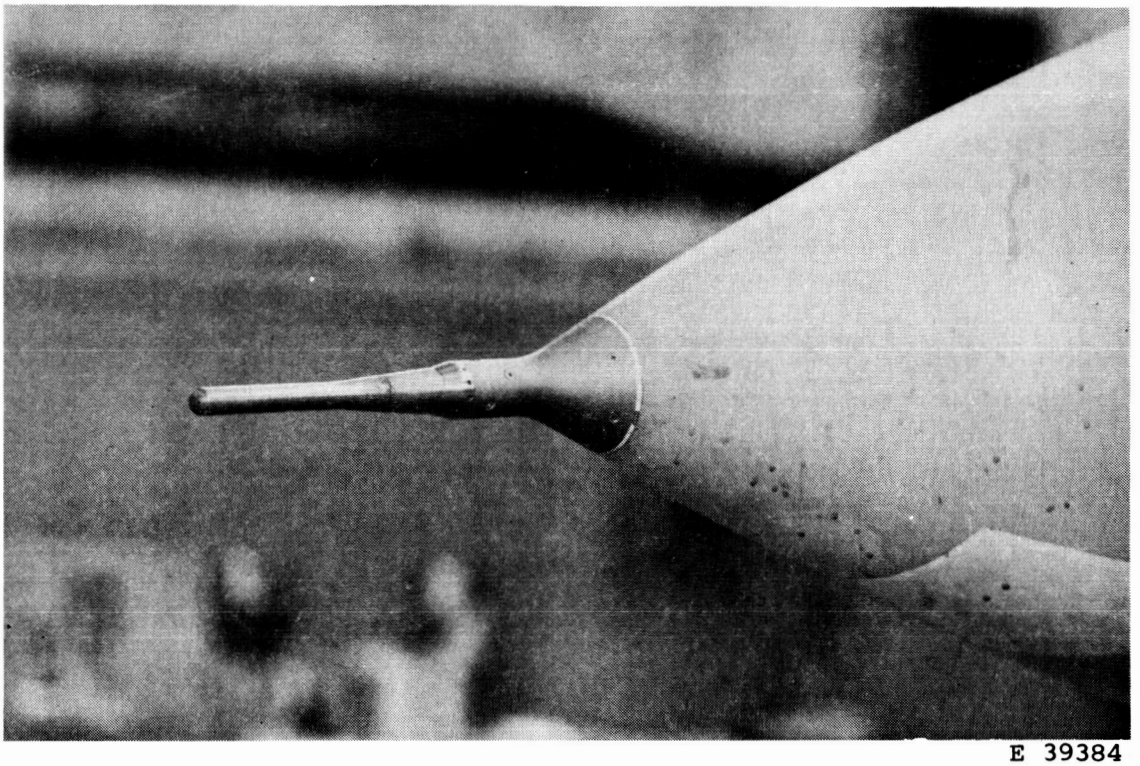

E 39384

Figure 1. ARI hemispherical flow-direction probe installed on F-14 nose.

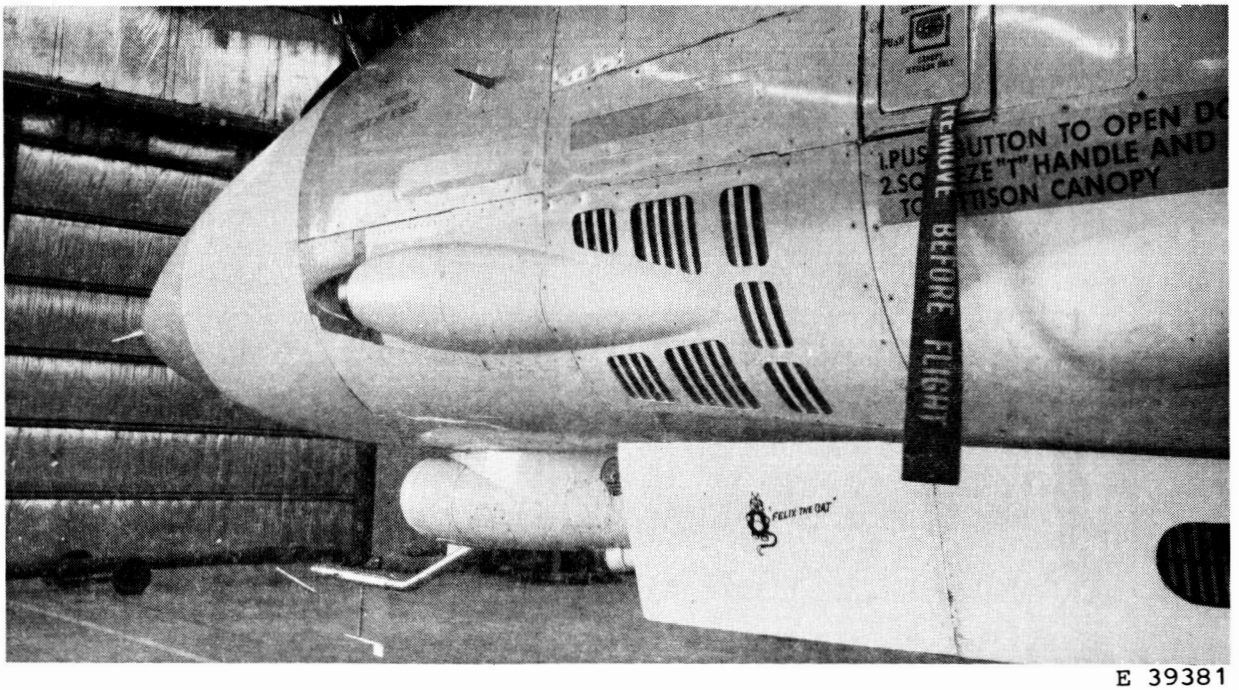

E 39381

Figure 2. AICS probe on left side of fuselage (gun fairing only on left side of fuselage).

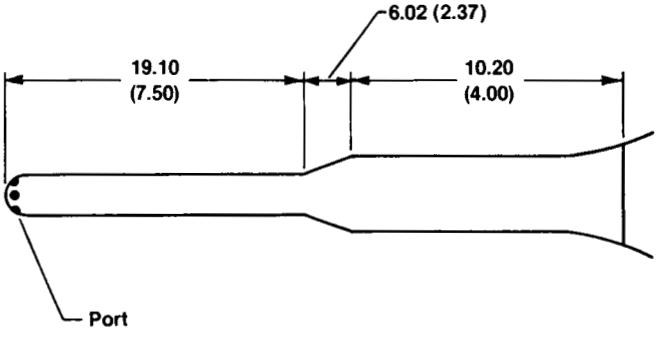

(a) ARI probe. Five parts are located on hemispherical surface (ref. 3).

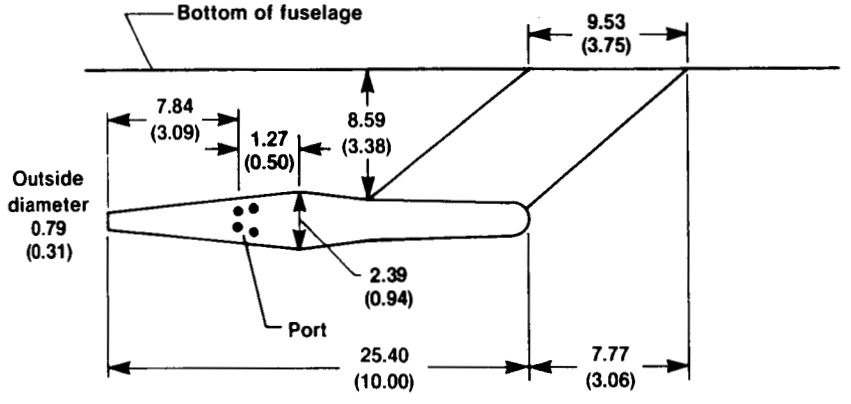

(b) AICS pitot-static probe. Four orifices are located in each row (two on top of probe and two on bottom). Orifices in forward row (S_1) are 0.318 cm (0.125 in) apart; orifices in row (S_2) are 0.64 cm (0.25 in) apart.

Figure 3. Test probes (top view). All dimensions are in cm (in).

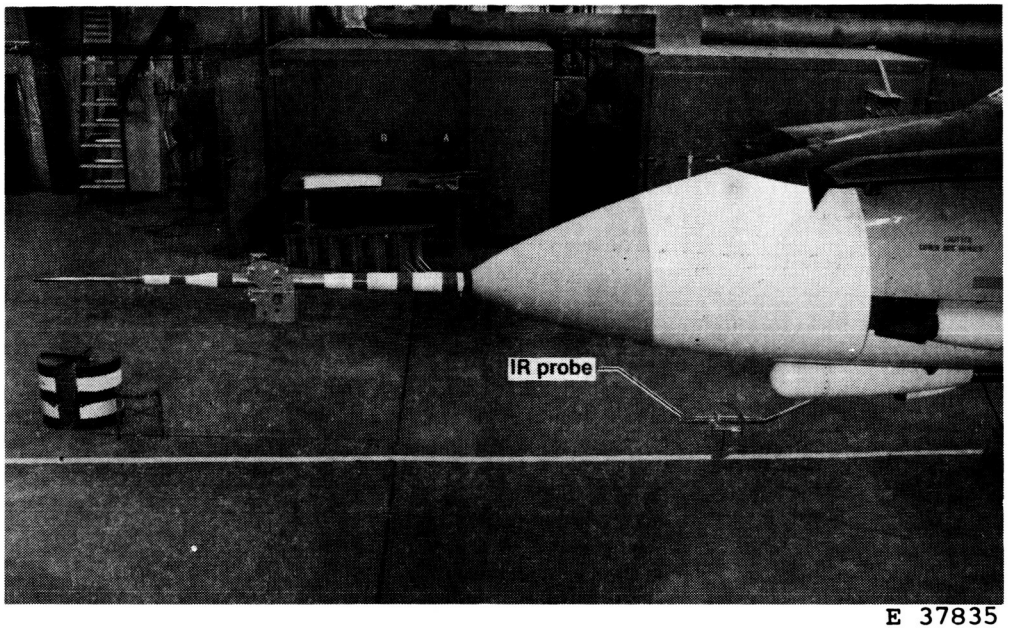

E 37835

Figure 4. Reference nose boom and IR-pod-mounted probes; protective guard and calibration jig installed on nose-boom probe and IR probe, respectively.

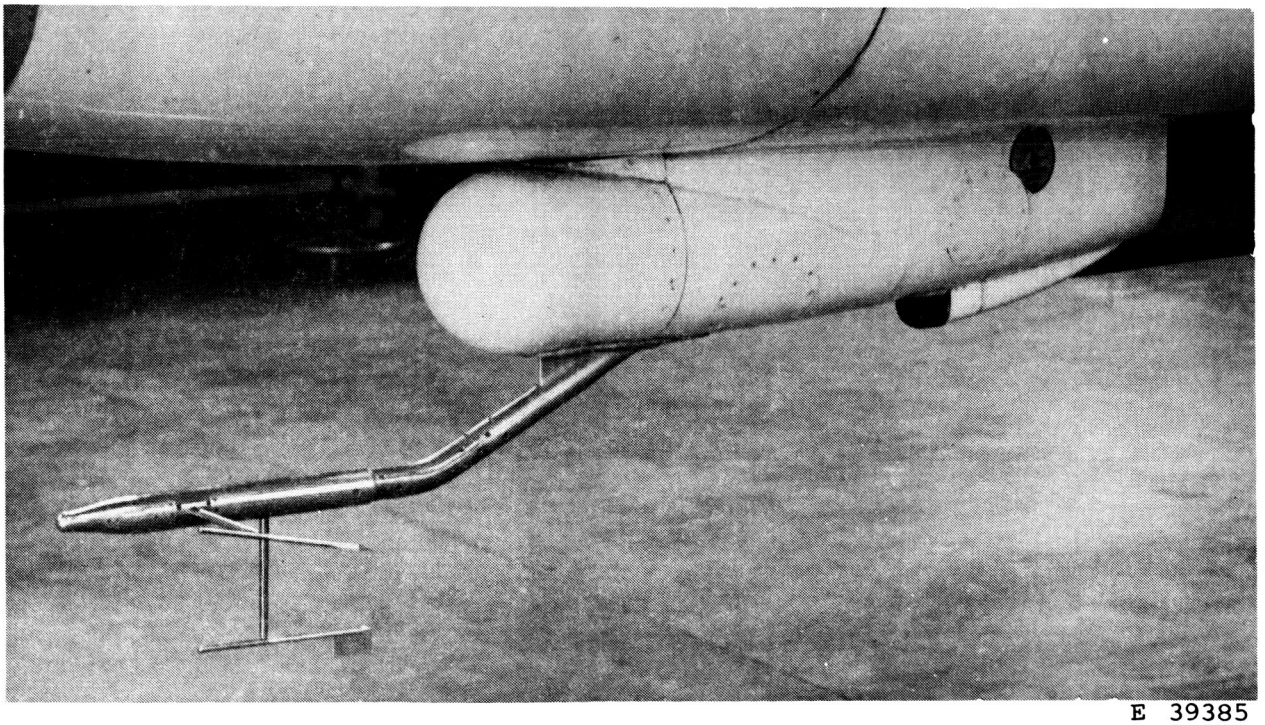

E 39385

Figure 5. IR-pod-mounted reference probe.

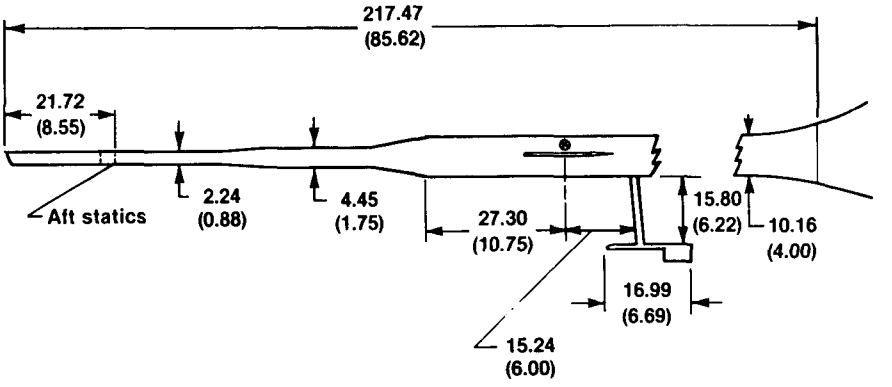

(a) Nose-mounted air-data probe.

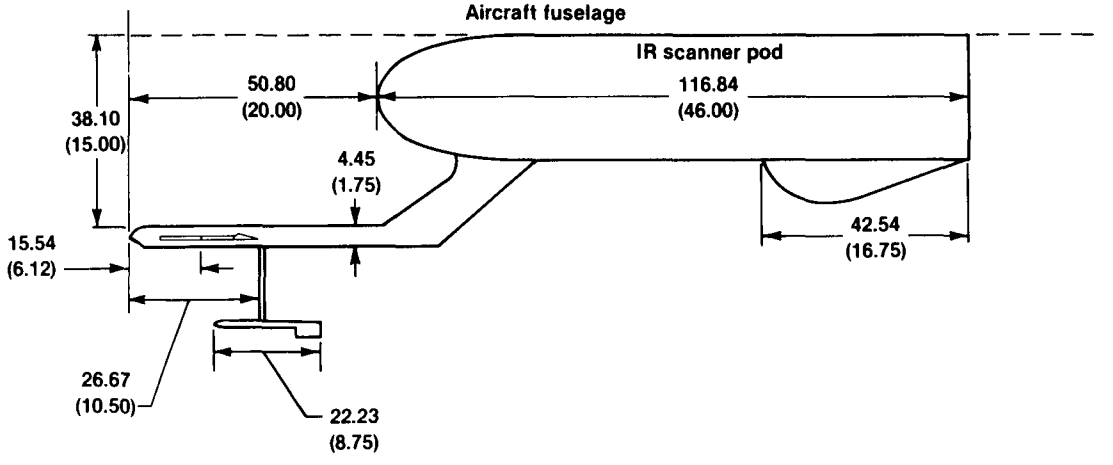

(b) Flow-direction probe mounted on IR scanner pod.

Figure 6. Reference air-data probes. All dimensions are in cm (in).

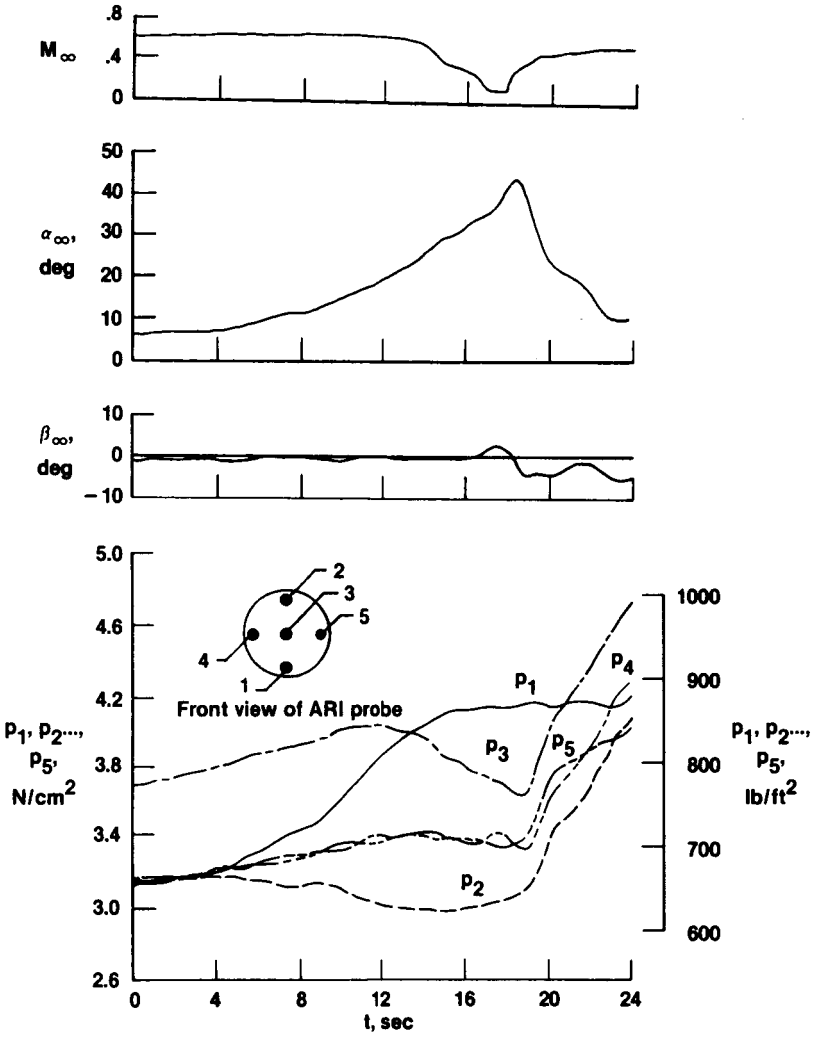

Figure 7. Time history of ARI probe pressures and aircraft reference quantities during angle-of-attack maneuver: $(M_\infty)_{max} = 0.64$.

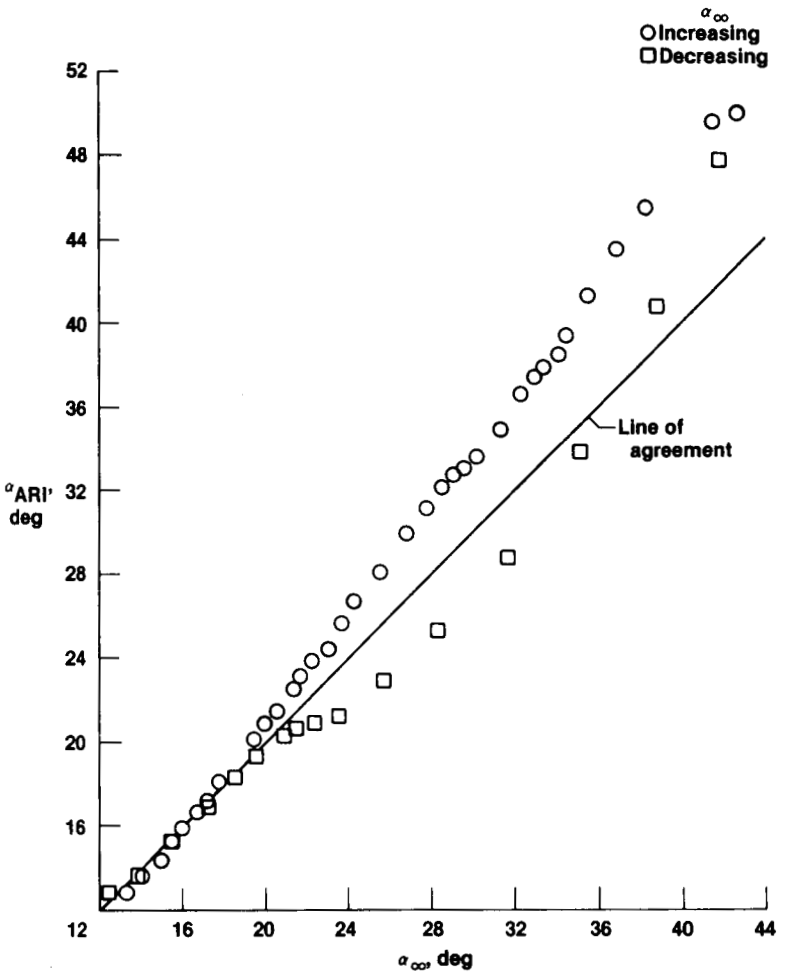

Figure 8. ARI probe angle of attack as a function of true angle of attack: $(M_\infty)_{max}$ = 0.64; 4 samples/sec.

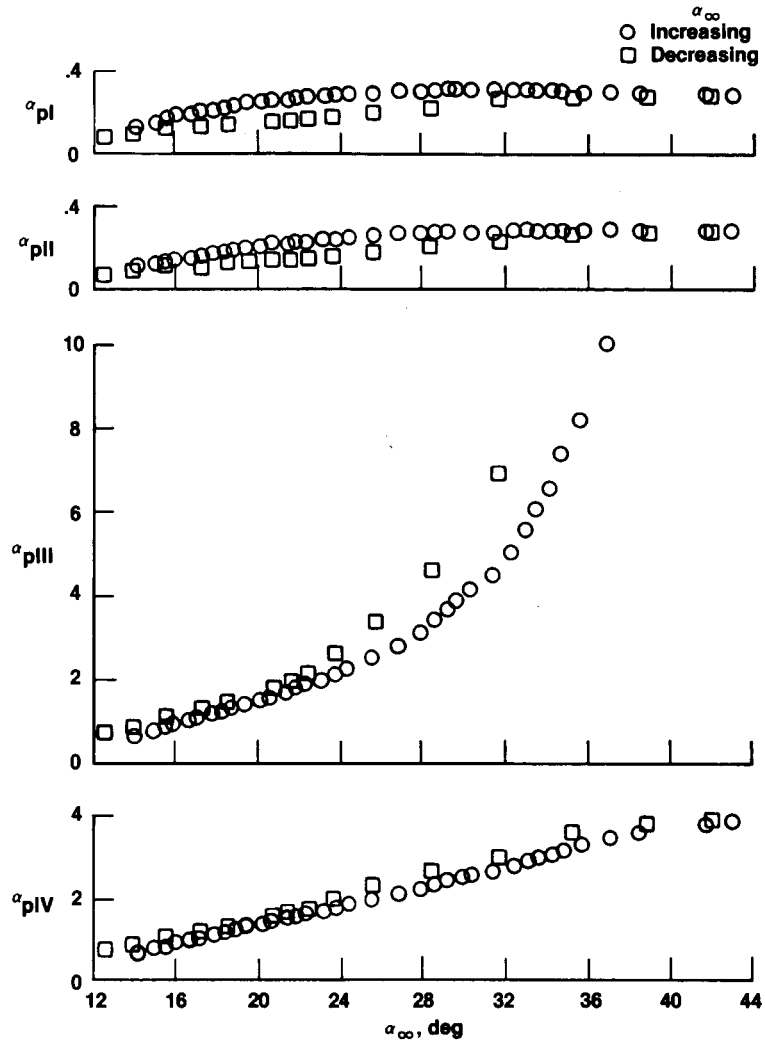

Figure 9. ARI probe angle-of-attack parameters as a function of true angle of attack: $(M_\infty)_{max}$ = 0.64; 4 samples/sec.

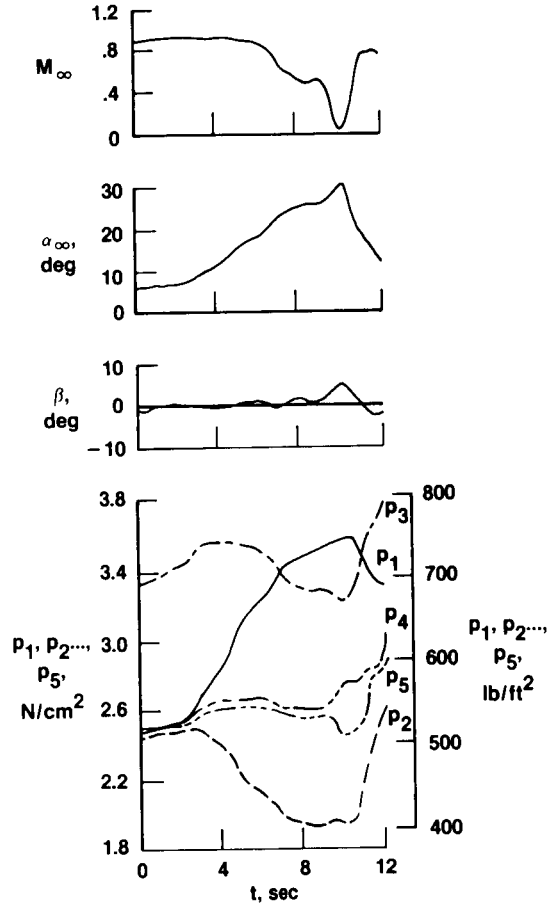

Figure 10. Time history of ARI probe and aircraft reference quantities during angle-of-attack maneuver: $(M_\infty)_{max}$ = 0.90.

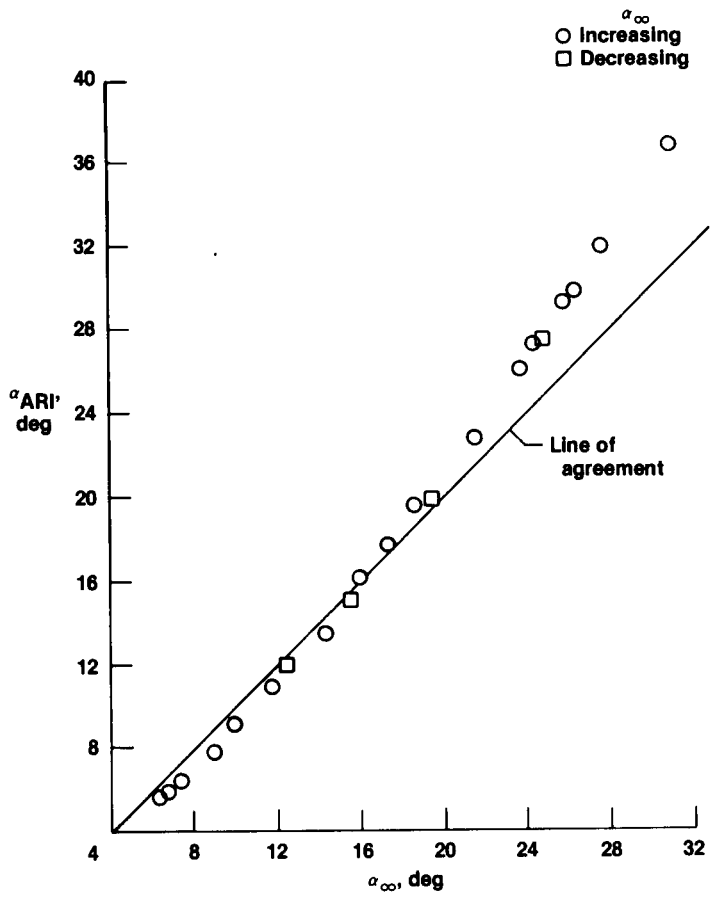

Figure 11. ARI probe angle of attack as a function of true angle of attack: $(M_\infty)_{max}$ = 0.90; 2 samples/sec.

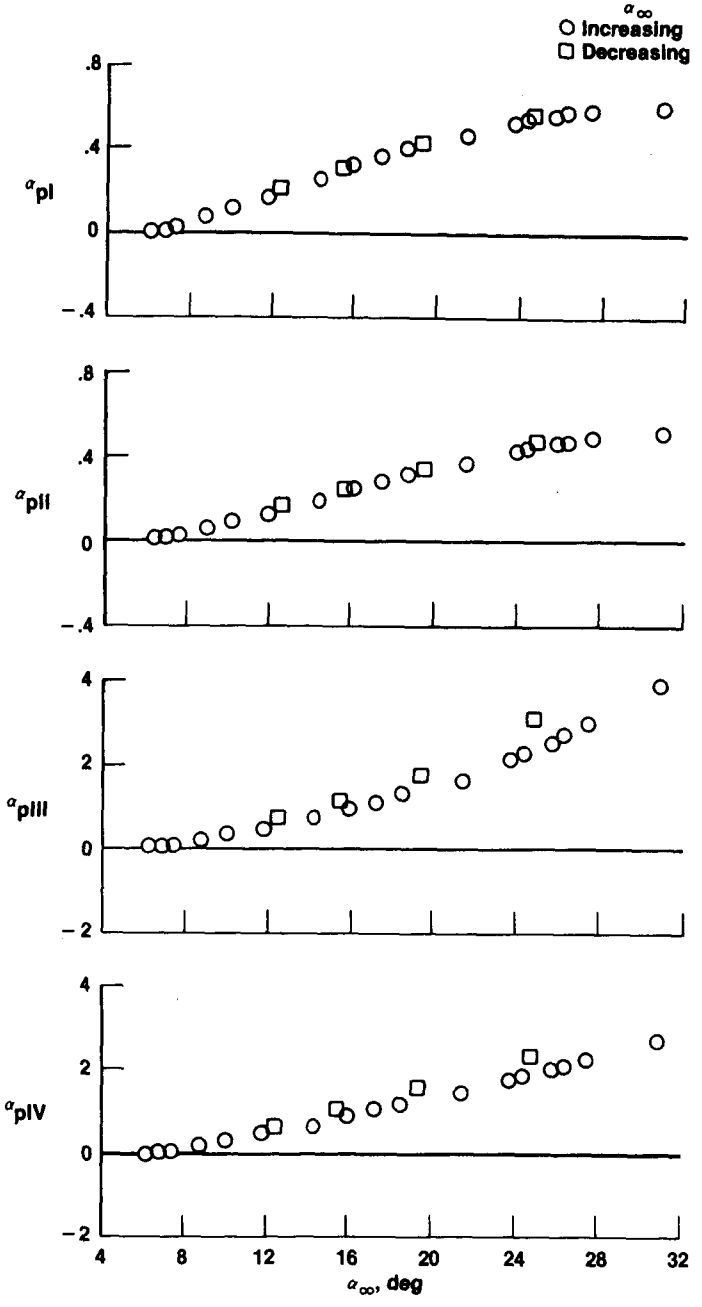

Figure 12. ARI probe angle-of-attack parameters as a function of true angle of attack: $(M_\infty)_{max}$ = 0.90; 2 samples/sec.

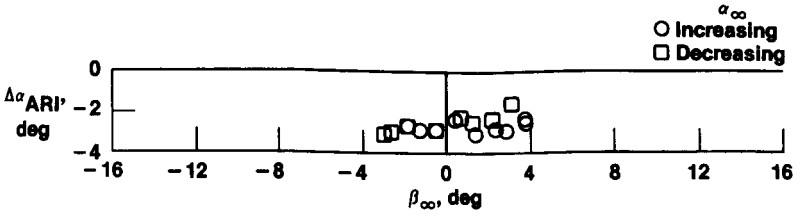

(a) α_∞ = 32° to 35°; M_∞ = 0.23 to 0.26.

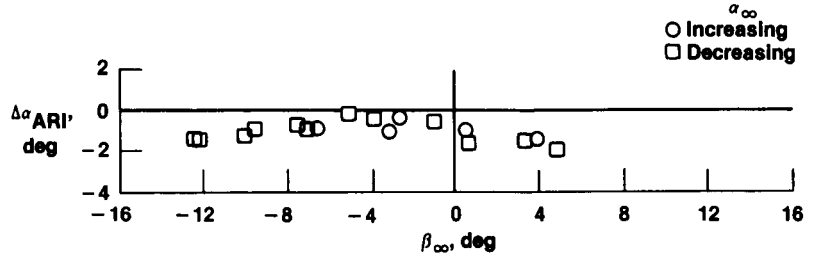

(b) α_∞ = 20° to 23°; M_∞ = 0.34 to 0.38.

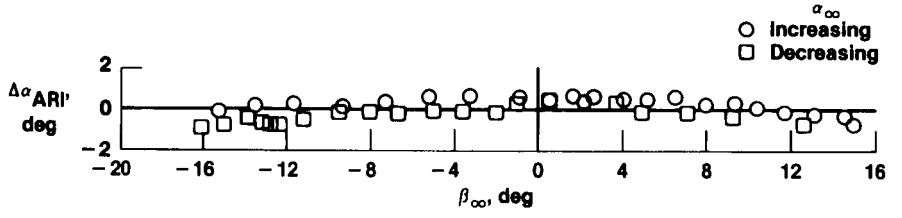

(c) α_∞ = 10° to 16°; M_∞ = 0.40 to 0.44.

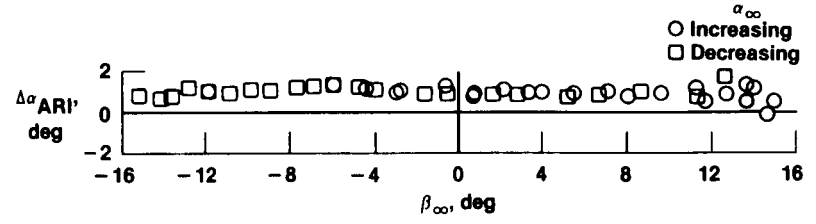

(d) α_∞ = 5° to 8°; M_∞ = 0.50 to 0.55.

Figure 13. ARI probe angle-of-attack correction as a function of angle of sideslip: low Mach number; 0.5 samples/sec.

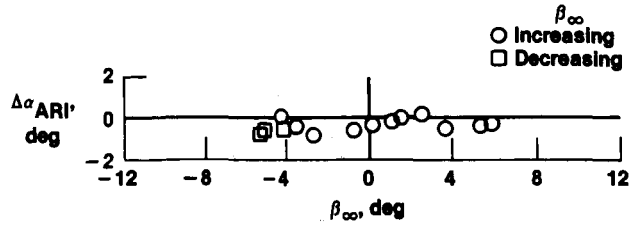

(a) α_∞ = 16° to 20°; M_∞ = 0.68 to 0.69.

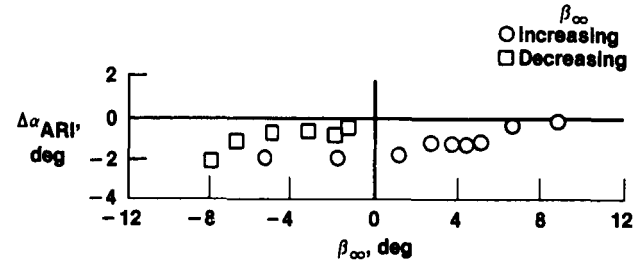

(b) α_∞ = 17° to 21°; M_∞ = 0.85 to 0.90.

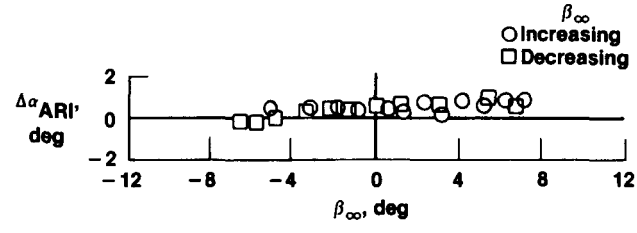

(c) α_∞ = 6° to 10°; M_∞ = 0.80 to 0.86.

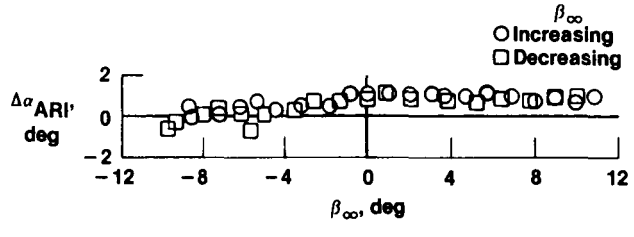

(d) α_∞ = 4° to 6°; M_∞ = 0.83 to 0.90.

Figure 14. ARI probe angle-of-attack correction as a function of true angle of sideslip: high Mach numbers.

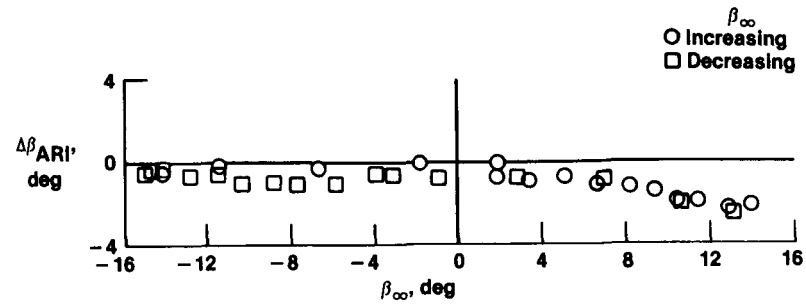

(a) α_∞ = 9° to 15°; M_∞ = 0.32 to 0.40; 1 sample/sec.

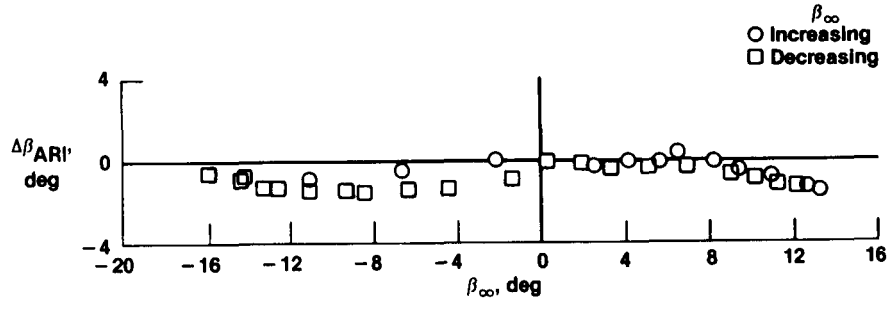

(b) α_∞ = 6° to 8°; M_∞ = 0.48 to 0.53; 0.5 sample/sec.

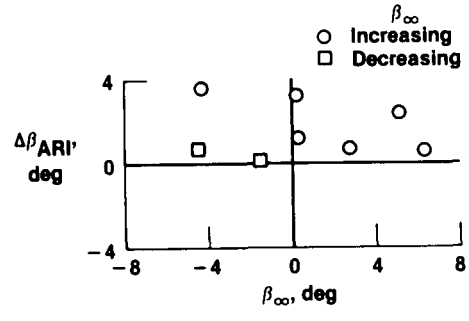

(c) α_∞ = 30° to 41°; M_∞ < 0.48; 2 sample/sec.

Figure 15. ARI probe angle-of-sideslip corrections as function of true angle of sideslip.

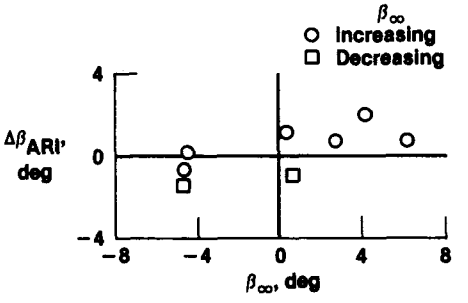

(d) α_∞ = 22° to 30°; M_∞ = 0.22 to 0.67; 2 sample/sec.

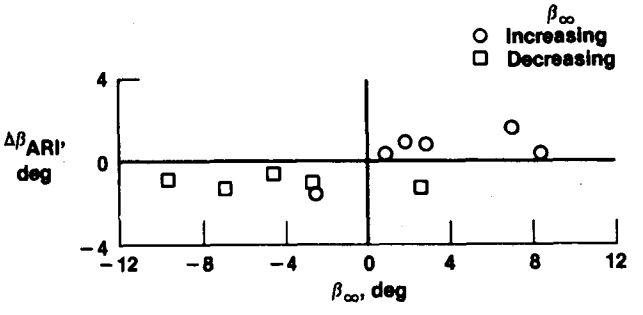

(e) α_∞ = 17° to 22°; M_∞ = 0.77 to 0.86; 2 sample/sec.

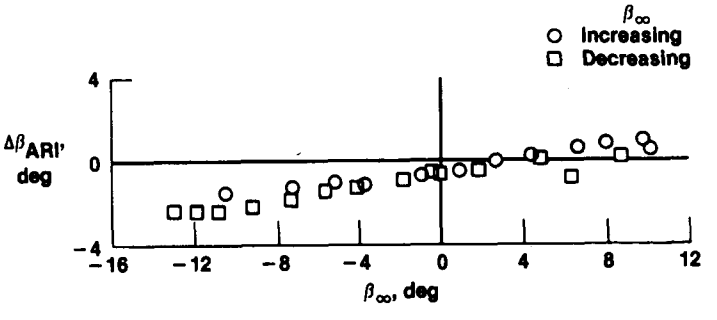

(f) α_∞ = 4° to 6°; M_∞ = 0.80 to 0.86; 2 sample/sec.

Figure 15. Concluded.

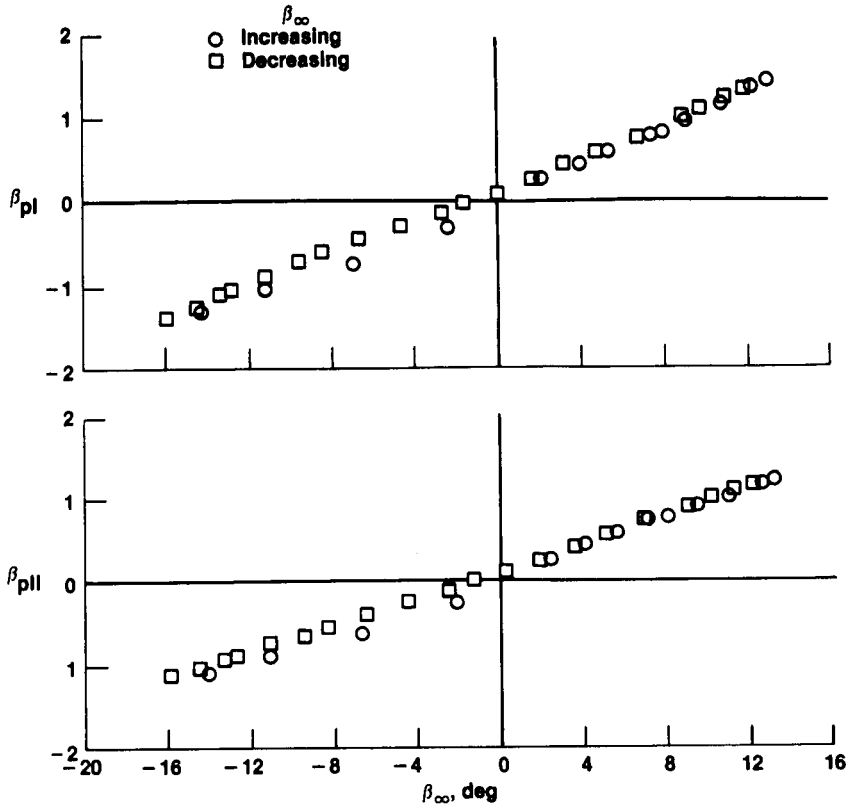

(a) Computed from data of figure 15(b).

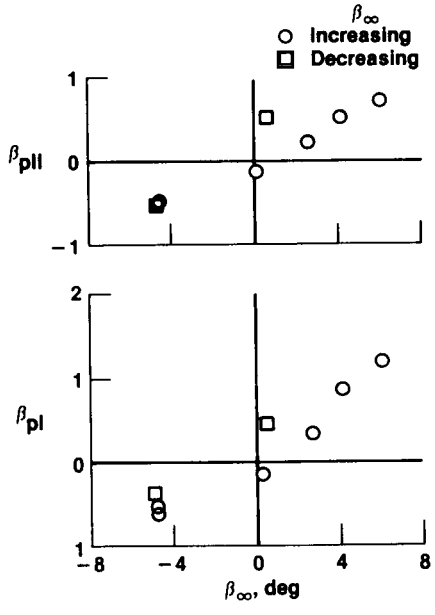

(b) Computed from data of figure 15(d).

Figure 16. ARI probe angle-of-sideslip parameters as a function of true angle of sideslip.

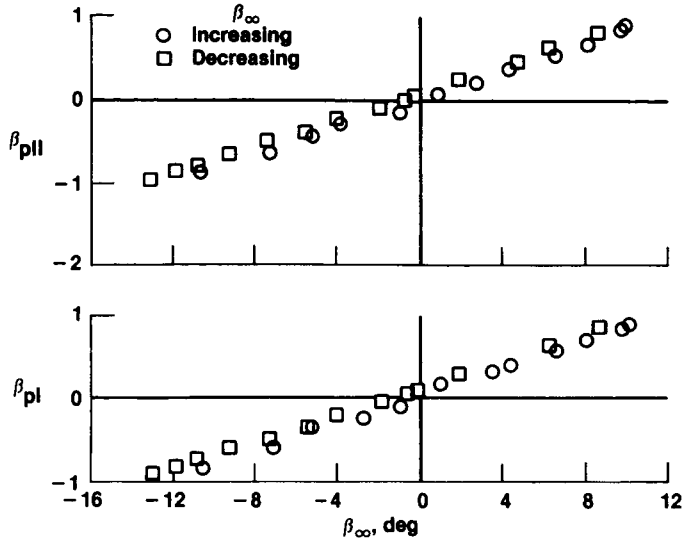

(c) Computed from data of figure 15(f).

Figure 16. Concluded.

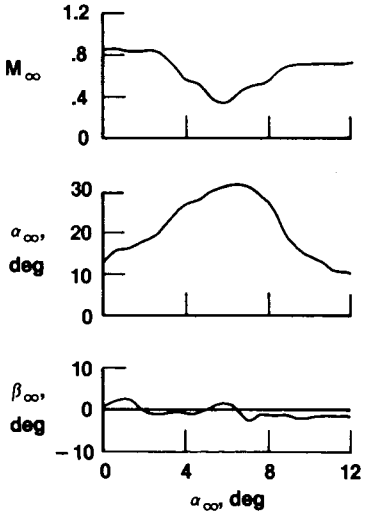

(a) Time history of angle-of-attack maneuver.

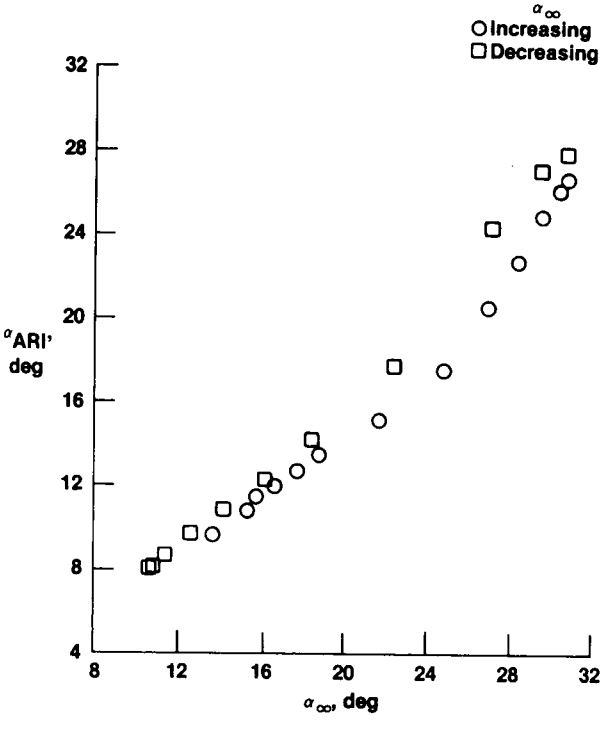

(b) ARI probe angle of attack as a function of true angle of attack; 2 samples/sec.

Figure 17. Angle-of-attack measurement performance of ARI probe mounted on IR pod; S_1 static pressure from AICS probe substituted for pneumatic averager.

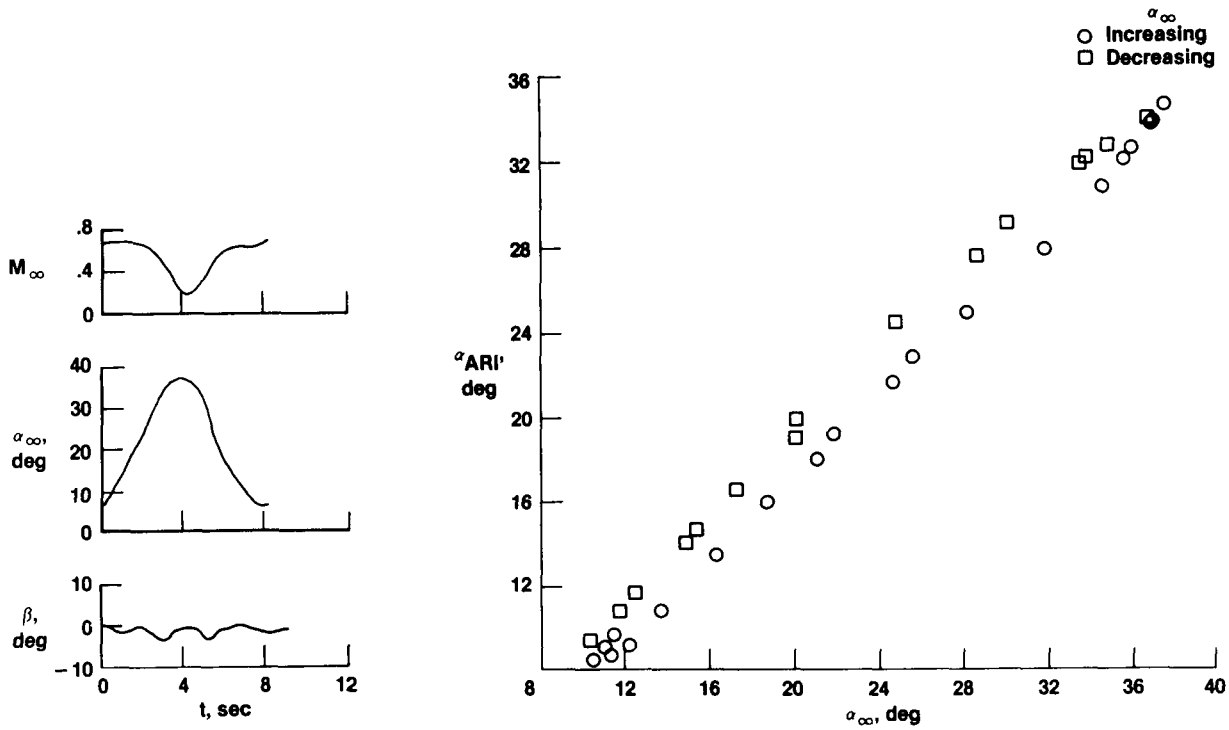

(a) Time history of angle-of-attack maneuver.

(b) ARI probe angle of attack as a function of true angle of attack: 4 samples/sec.

Figure 18. Angle-of-attack measurement performance of ARI probe mounted on IR pod; ports 3 and 4 manifolded and substituted for pneumatic averager.

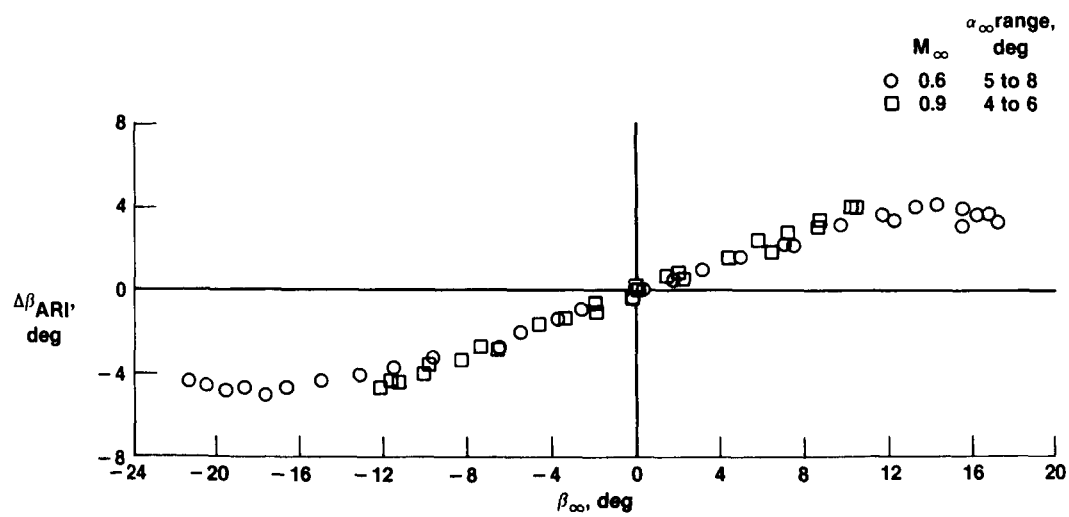

Figure 19. Angle-of-sideslip measurement performance of ARI probe mounted on IR pod; S_1 static pressure from AICS probe substituted for pneumatic averager.

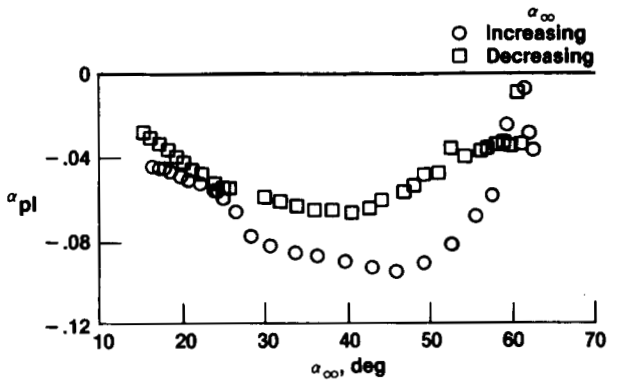

(a) α_{pII} parameter.

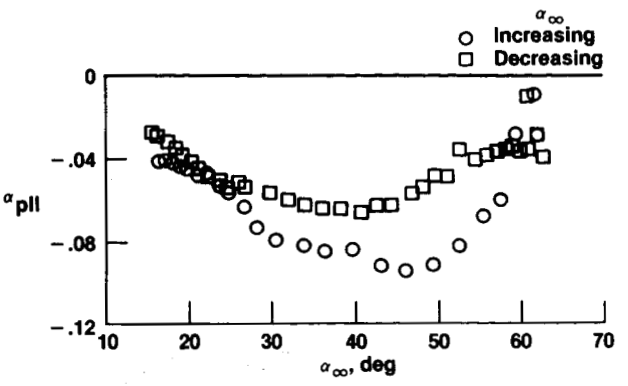

(b) α_{pI} parameter.

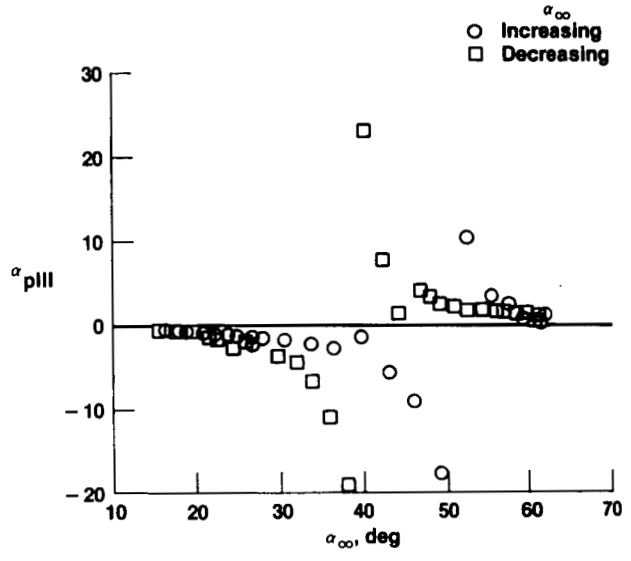

(c) α_{pIII} parameter.

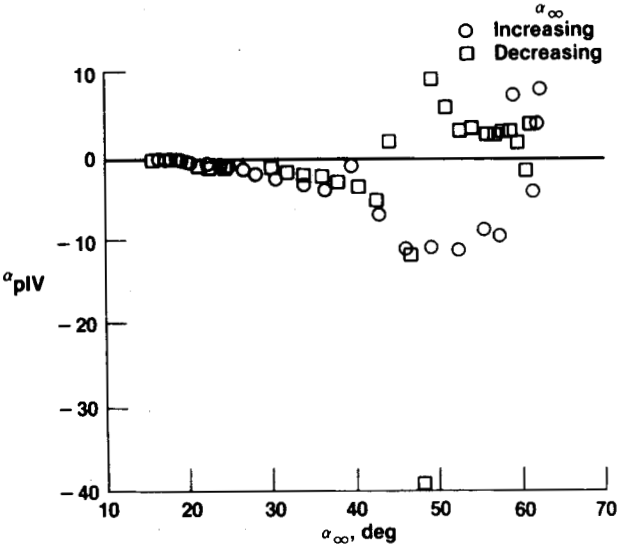

(d) α_{pIV} parameter.

Figure 20. Angle-of-attack parameters computed for ARI probe mounted on IR pod as a function of true angle of attack: pneumatic averager installed, $M_\infty < 0.4$, 10 samples/sec.

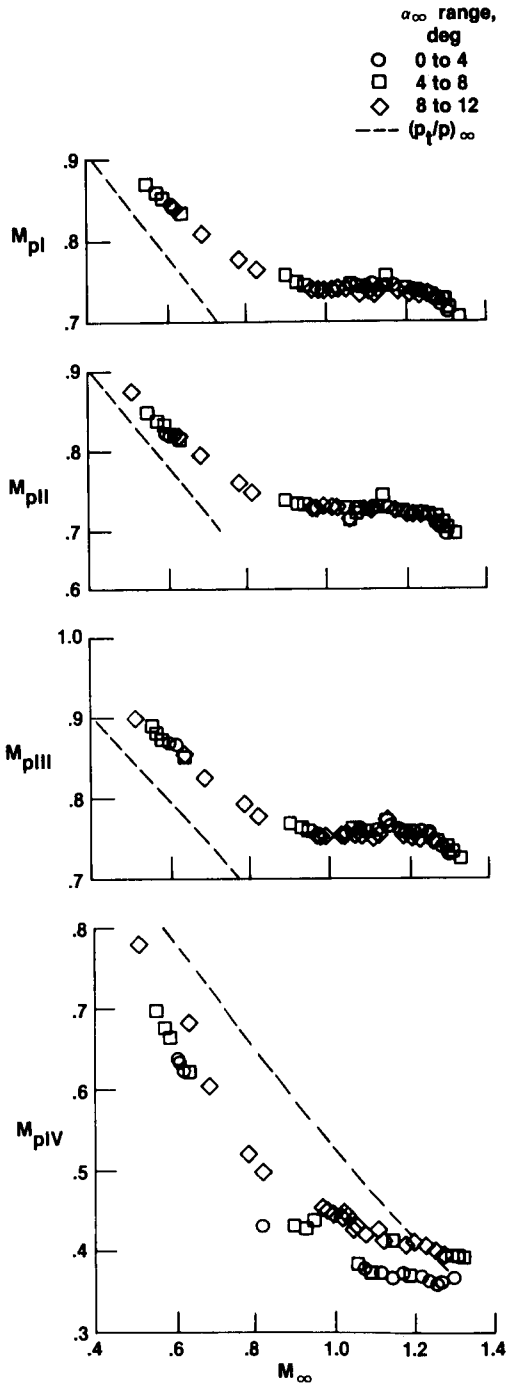

Figure 21. Mach number parameters computed for ARI probe mounted on IR pod as a function of Mach number; pneumatic averager installed.

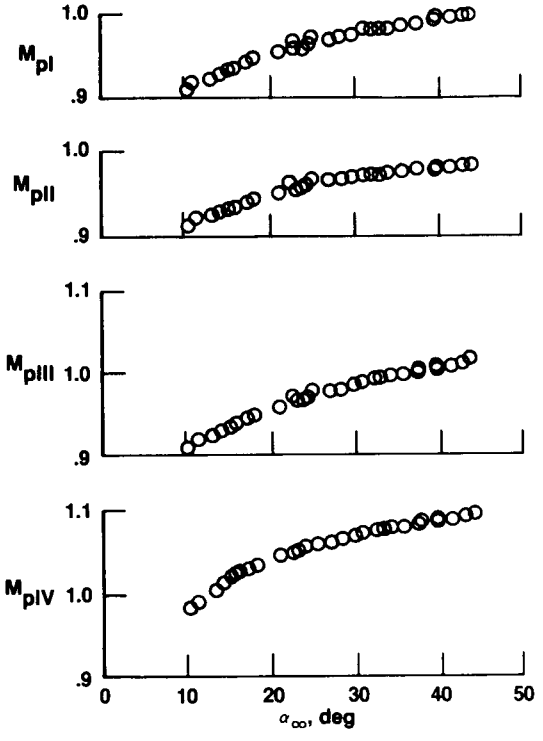

Figure 22. Mach number parameters computed for ARI probe mounted on IR pod as a function of true angle of attack: pneumatic averager installed, $M_\infty \approx 0.4$.

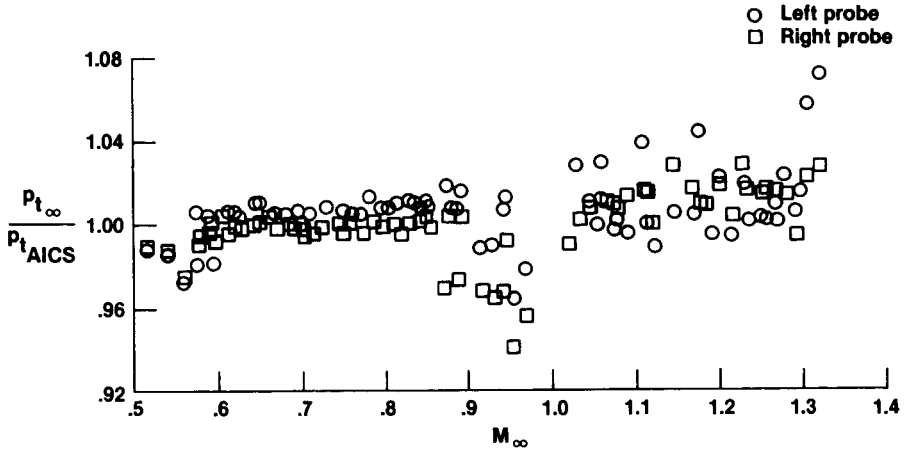

(a) Stagnation pressure.

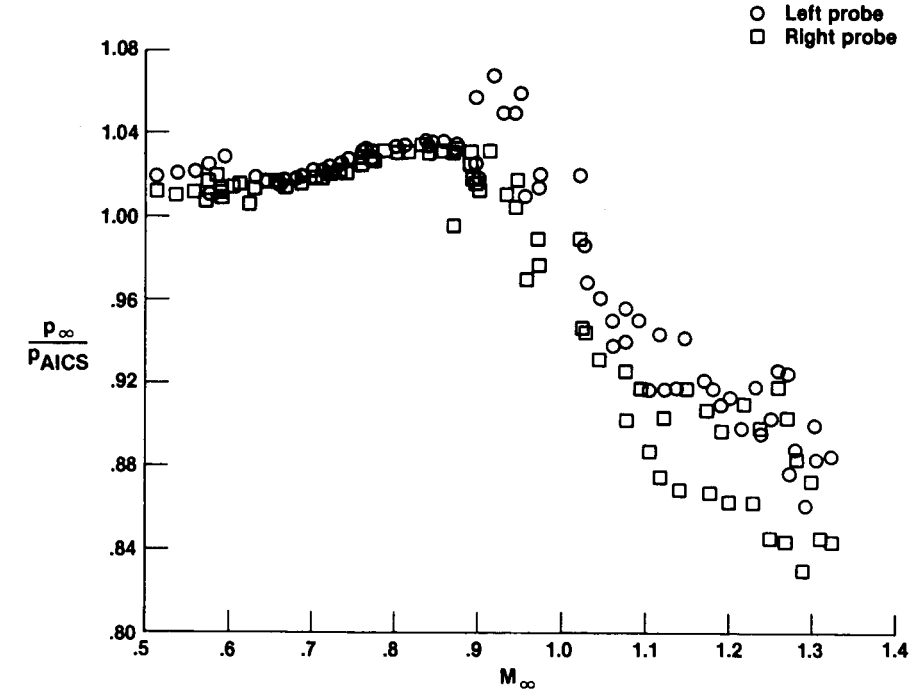

(b) Static pressure, S_2 source.

Figure 23. Stagnation-pressure and static-pressure performance of AICS probes as a function of true Mach number: $\alpha_\infty < 14°$.

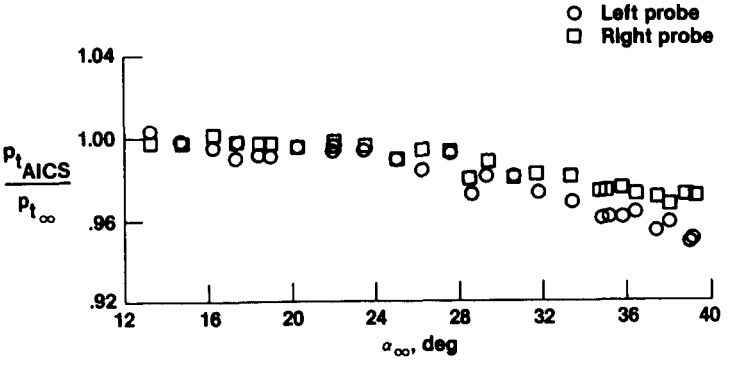

(a) Stagnation pressure.

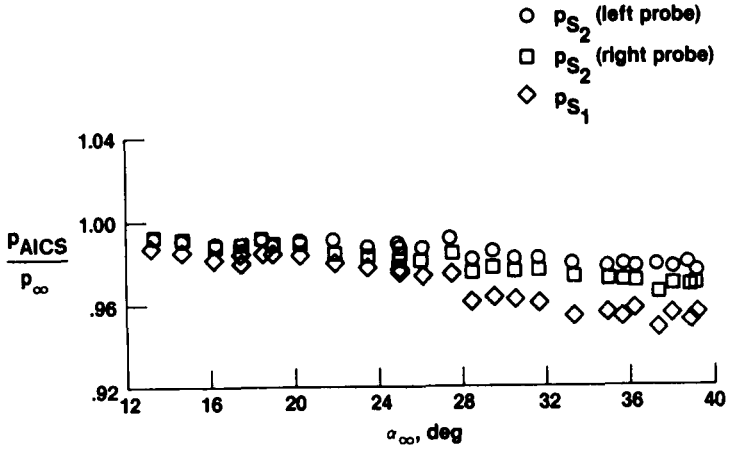

(b) Static pressure.

Figure 24. Stagnation-pressure and static-pressure performance of AICS probes as a function of angle of attack: $M_\infty \approx 0.3$.

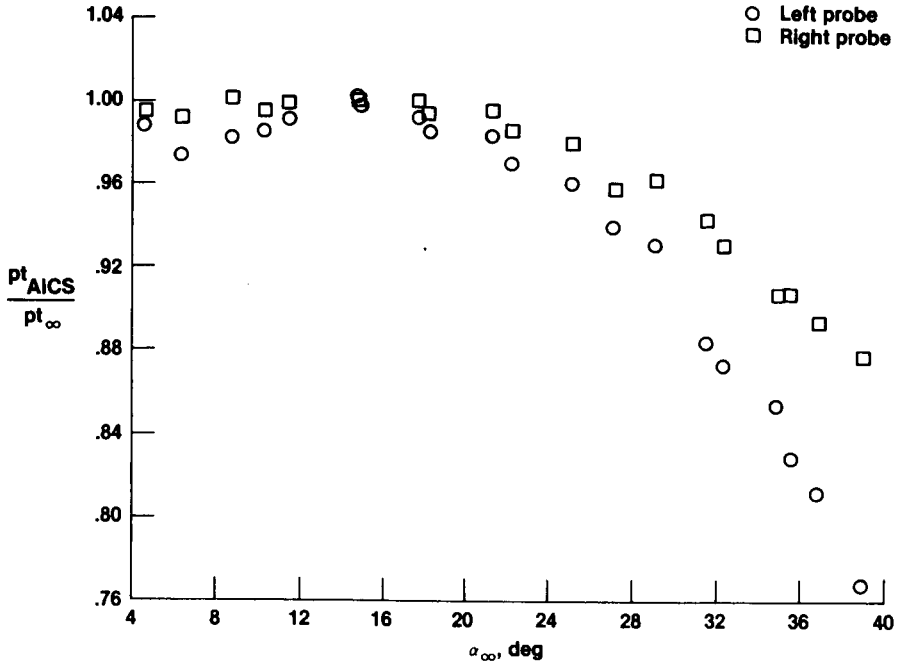

(a) Stagnation pressure.

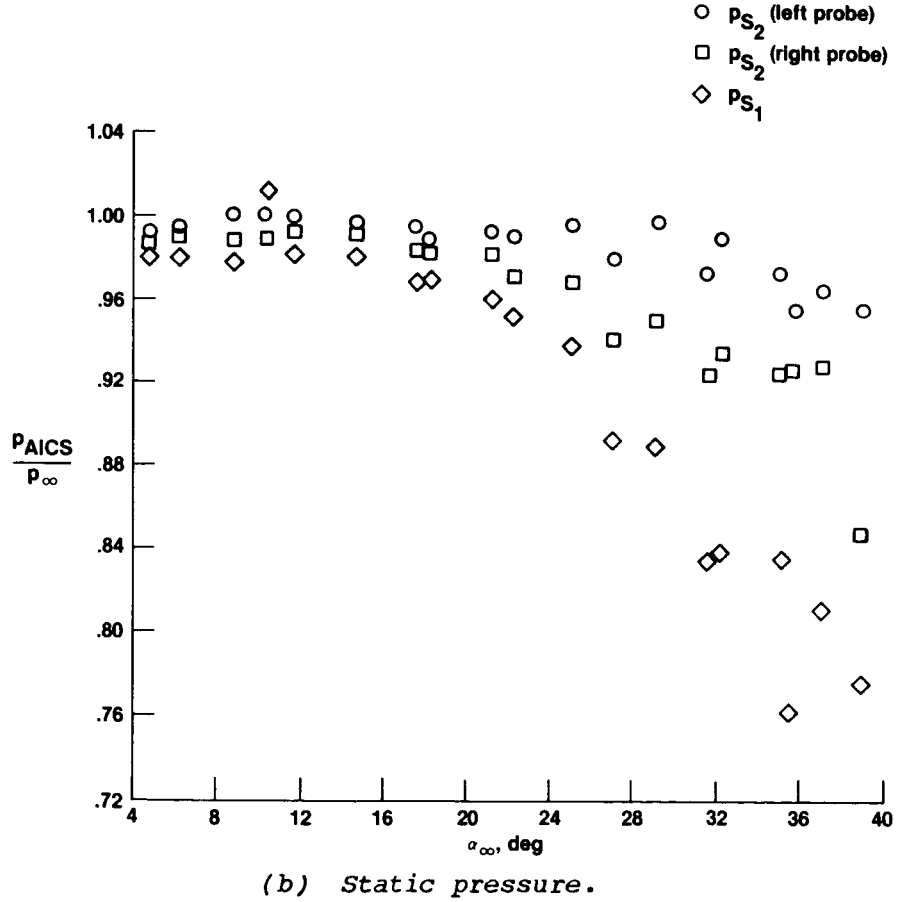

(b) Static pressure.

Figure 25. Stagnation-pressure and static-pressure performance of AICS probes versus true angle of attack: $M_\infty \approx 0.6$.

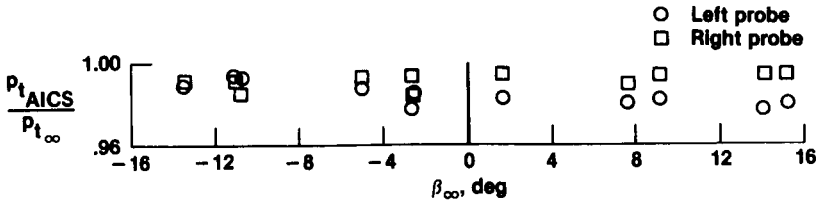

(a) Stagnation pressure.

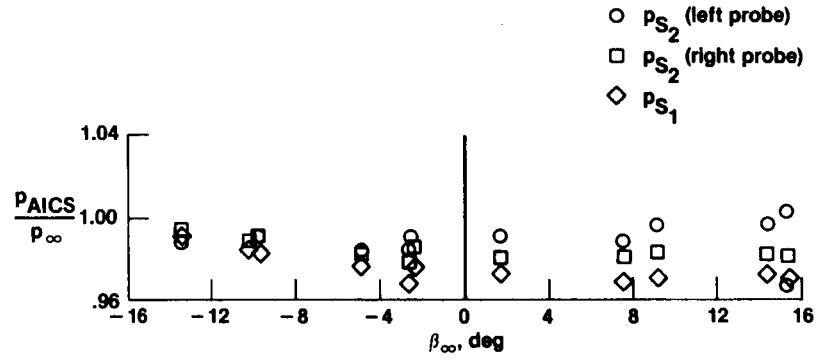

(b) Static pressure.

Figure 26. Stagnation pressure and static pressure performance of AICS probes as a function of true angle of sideslip: $M_\infty \approx 0.3$.

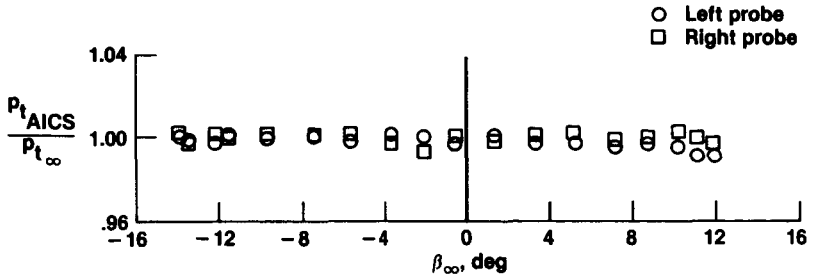

(a) Stagnation pressure.

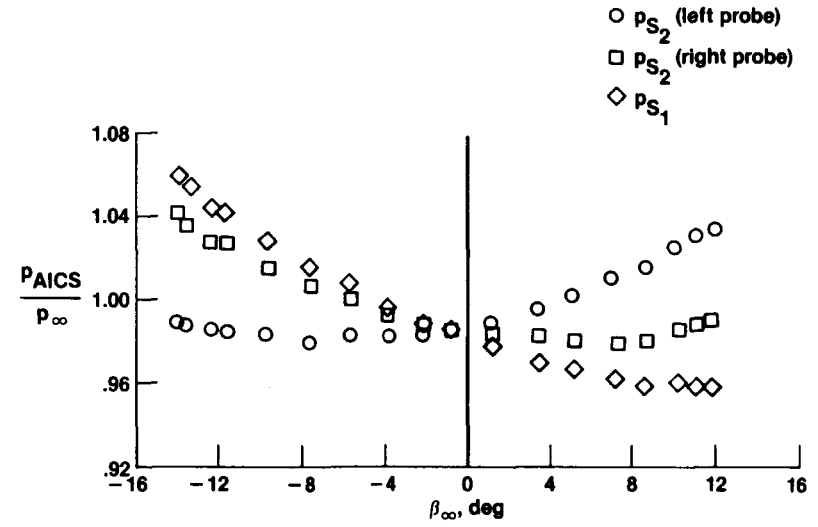

(b) Static pressure.

Figure 27. Stagnation-pressure and static-pressure performance of AICS probes as a function of true angle of sideslip: $M_\infty \approx 0.6$.

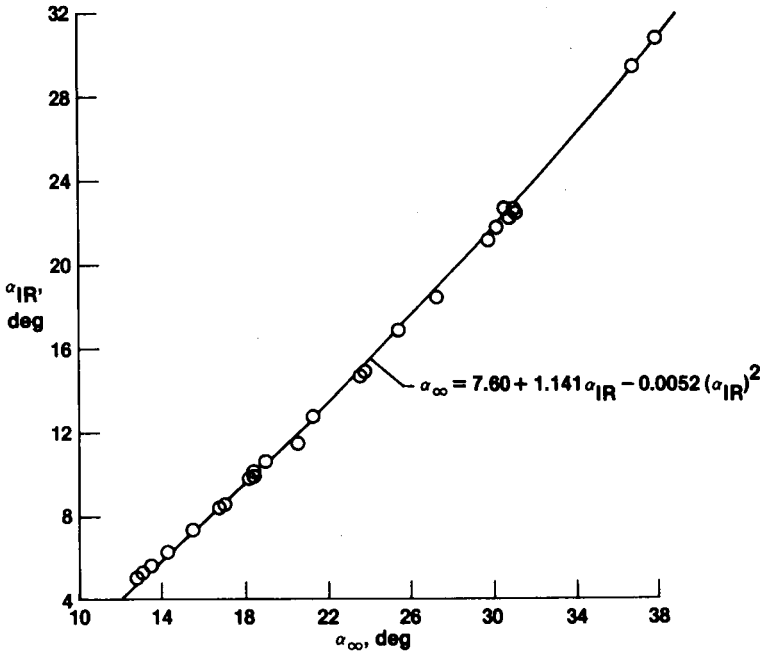

Figure 28. IR-pod-mounted probe angle of attack as a function of true angle of attack: $M_\infty \approx 0.3$, $\beta_{IR} \approx 0$.

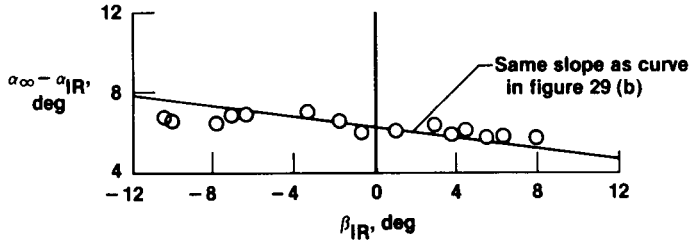

(a) $\alpha_\infty \approx 32°$.

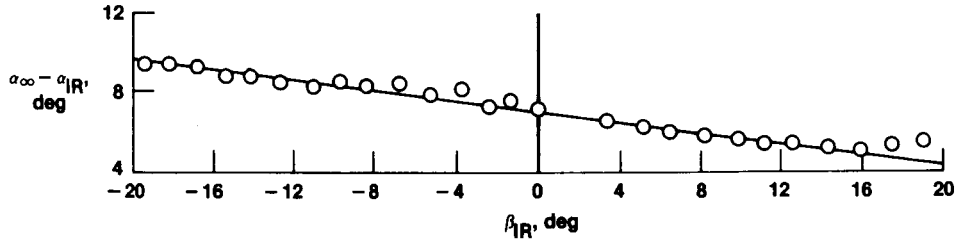

(b) $\alpha_\infty \approx 3°$.

Figure 29. IR-pod-mounted probe angle of attack as a function of IR probe angle of sideslip: low M_∞.

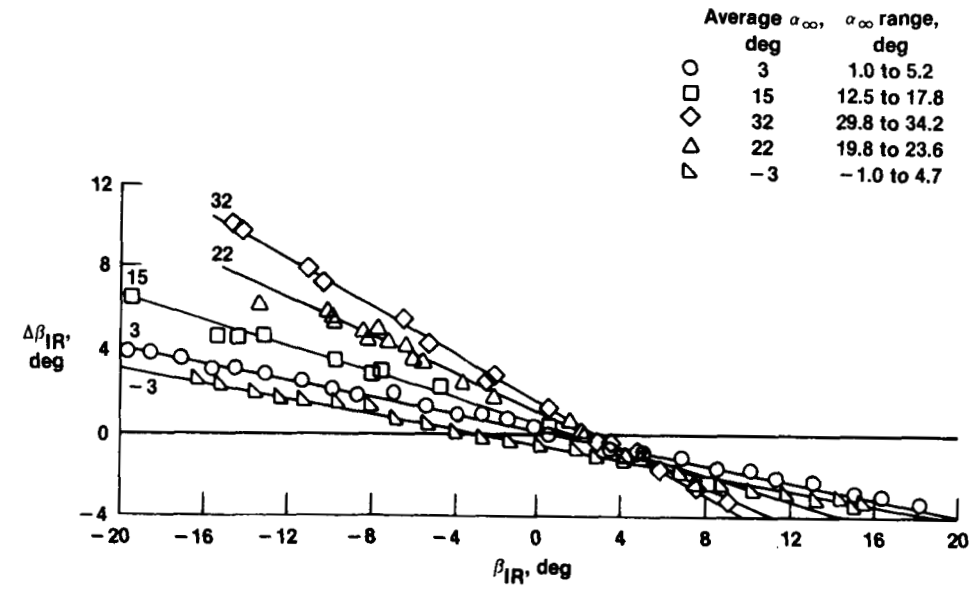

Figure 30. IR-pod-mounted probe sideslip correction as a function of IR angle of sideslip. $M_\infty \approx 0.3$.

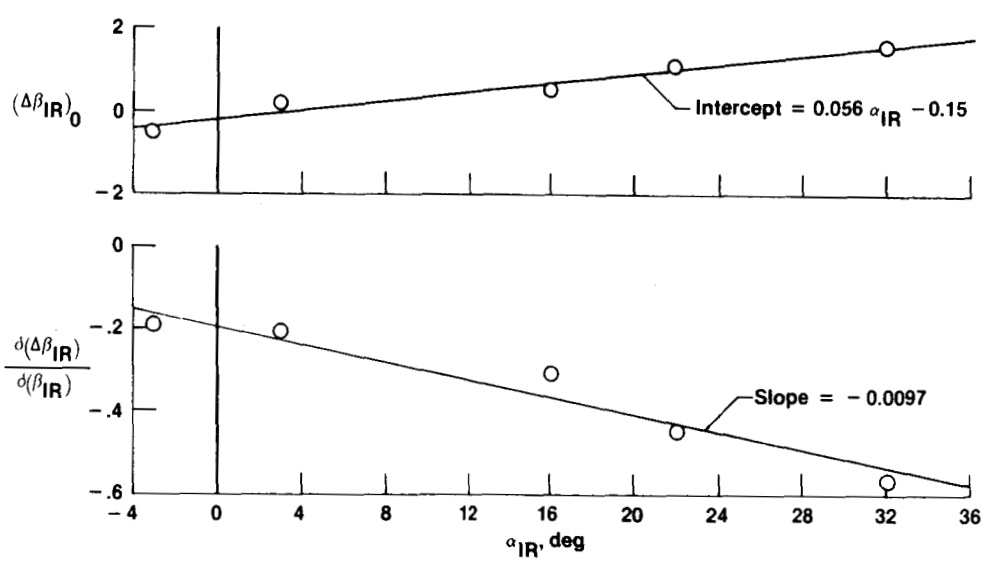

Figure 31. Variation of intercept and slope calibration factors with IR-probe angle of attack for IR-sideslip vane: $M_\infty \approx 0.3$.

1. Report No. NASA TM-84911	2. Government Accession No.	3. Recipient's Catalog No.

4. Title and Subtitle	5. Report Date
Evaluation of a Flow Direction Probe and a Pitot-Static Probe on the F-14 Airplane at High Angles of Attack and Sideslip	March 1984
	6. Performing Organization Code
7. Author(s) Terry J. Larson	8. Performing Organization Report No. H-1189
	10. Work Unit No.
9. Performing Organization Name and Address NASA Ames Research Center Dryden Flight Research Facility P.O. Box 273 Edwards, California 93523	11. Contract or Grant No.
	13. Type of Report and Period Covered Technical Memorandum
12. Sponsoring Agency Name and Address National Aeronautics and Space Administration Washington, D.C. 20546	14. Sponsoring Agency Code RTOP 505-31-21

15. Supplementary Notes

16. Abstract

The measurement performance of a hemispherical flow-angularity probe and a fuselage-mounted pitot-static probe has been evaluated at high flow angles as part of a test program on an F-14 airplane. These evaluations were performed using a calibrated pitot-static noseboom equipped with vanes for reference flow direction measurements, and another probe incorporating vanes but mounted on a pod under the fuselage nose. Data are presented for angles of attack up to 63°, angles of sideslip from -22° to 22°, and for Mach numbers from approximately 0.3 to 1.3.

During maneuvering flight, the hemispherical flow-angularity probe exhibited flow angle errors that exceeded 2°. Pressure measurements with the pitot-static probe resulted in very inaccurate data above a Mach number of 0.87 and exhibited large sensitivities with flow angle.

17. Key Words (Suggested by Author(s))	18. Distribution Statement
Air data Angle of attack Angle of sideslip Pitot-static measurements Airspeed	Unclassified-Unlimited STAR category 05

19. Security Classif. (of this report)	20. Security Classif. (of this page)	21. No. of Pages	22. Price*
Unclassified	Unclassified	39	A03

*For sale by the National Technical Information Service, Springfield, Virginia 22161.